

# 國立交通大學

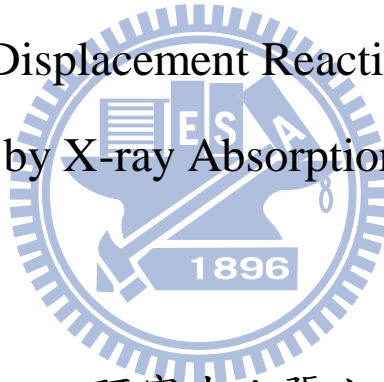
加速器光源科技與應用碩士學位學程

碩士論文

利用 X 光吸收光譜研究鉑原子在鈦奈米顆粒的置換反應

Investigation of Displacement Reaction for Pt on Ru/C

Nanoparticles by X-ray Absorption Spectroscopy



研究生：張立忠

指導教授：吳樸偉 教授

李志甫 博士

中華民國九十九年七月

# National Chiao Tung University

## Graduate Program for Science and Technology of Accelerator Light Source

### Thesis

利用 X 光吸收光譜研究鉑原子在鈦奈米顆粒的置換反應

Investigation of Displacement Reaction for Pt on Ru/C

Nanoparticles by X-ray Absorption Spectroscopy

Student: Li-Chung Chang

Advisors: Prof. Pu-Wei Wu

Dr. Jyh-Fu Lee

July, 2010

# 利用 X 光吸收光譜研究鉑原子在鈎奈米顆粒的置換反應

研 究 生：張立忠

Student : Li-Chung Chang

指 導 教 授：吳樸偉 教授

Advisor : Prof. Pu-Wei Wu


李志甫 博士

Dr. Jyh-Fu Lee

國立交通大學

加速器光源科技與應用碩士學位學程

碩士論文



A Thesis  
Submitted to Graduate Program for Science and Technology of Accelerator Light Source  
College of Engineering  
National Chiao Tung University  
in partial Fulfillment of the Requirements  
for the Degree of  
Master  
in

Graduate Program for Science and Technology of Accelerator Light Source

July 2010

Hsinchu, Taiwan, Republic of China

中華民國九十九年七月

# 利用 X 光吸收光譜研究鉑原子在鈦奈米顆粒的置換反應

研究生：張立忠

指導教授：吳樸偉 博士

李志甫 博士

國立交通大學加速器光源科技與應用碩士學位學程

## 摘要

置換反應為一個新穎的觸媒製備方式，對於直接甲醇燃料電池陽極或陰極觸媒都有相關的應用。該方法解決了傳統觸媒製備時遭遇的問題，例如貴重金屬的乘載量太高和使用率太低。利用置換反應所製備的觸媒可以降低貴重金屬的承載量到單一原子層或甚至更低。可以提升貴重金屬參與觸媒反應的使用率，減少貴重金屬的浪費便可以降低燃料電池系統單價。然而，置換反應的反應機制相當複雜，需要投入更多的研究加以釐清。藉由增加對反應過程的基礎知識，使得置換反應所製備出來的觸媒得以最佳化。

在本研究中，置換反應中所參與的元素為鉑與鈦。選擇這兩個元素做為研究對象的原因，除了鉑鈦合金之間會進行置換反應外，鉑鈦合金也是一個效能優異的直接甲醇燃料電池陽極觸媒。首先，我們使用化學還原法製備的碳承載之鈦奈米顆粒，緊接著將他們浸泡入鉑的前驅物中進行置換反應後進行分析。並且，在不同酸鹼值下的鉑前驅物，對於鈦的置換反應中的影響也進行深入的探討。研究方法主要使用 X 光吸收光譜來鑑定置換反應過程中，鉑的氧化價數和微結構變化情形。同時，鈦的氧化價數和微結構變化也進行分析，使得我們可以分別用鉑與鈦的變化建構一個合理的反應機制。另一方面，由穿透式電子顯微鏡得知鈦奈米顆粒均勻分布在碳的承載物上，並且置換上鉑之後的顆粒大小並沒有明顯的變化；X 光繞射圖顯示鈦受到了鉑的影響，晶格有變大的情形；能量分散 X 光譜儀和感應耦合電漿質譜分析儀指出置換反應中，鉑的沉積量和鈦被置換的量受鉑前驅物酸鹼值有相當的影響。

總結以上分析結果，利用置換反應將鉑沉積在鈦奈米顆粒的反應過程中：鉑離子被鈦還原至較低的氧化價數並沉積在鈦奈米顆粒的表面，而鈦氧化成離子並解離入前驅物水溶液當中。然而，鉑並非直接與鈦形成鍵結，是藉由氧的嫁接形成鍵結在鈦的表面。



# **Investigation of Displacement Reaction for Pt on Ru/C Nanoparticles by X-ray Absorption Spectroscopy**

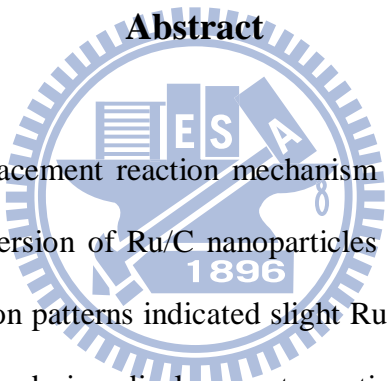
Student: Li-Chung Chang

Advisors: Prof. Pu-Wei Wu

Dr. Jyh Fu Lee

Graduate Program for Science and Technology of Accelerator Light Source  
National Chiao Tung University

## **Abstract**



An investigation to the displacement reaction mechanism for Pt on Ru/C nanoparticles was carried out by analyzing the immersion of Ru/C nanoparticles into hexachloroplatinic acids with various pH values. X-ray diffraction patterns indicated slight Ru lattice expansion of Pt deposition. The exact variation of Pt and Ru during displacement reaction was determined by inductively coupled plasma mass spectrometry, which suggested that the dissolution of Ru was mainly resulted from the displacement by Pt. The Ru/C and PtRu/C were approximately 2 to 3 nm in sizes from TEM images from transmission electron microscope. Energy dispersive x-ray spectroscopy determined the composition of Pt on Ru nanoparticles. X-ray absorption spectroscopy analysis provided a detailed reaction mechanism which indicated that Pt cations were reduced to moderate oxidation states or merely physically adsorbed contingent on the types of complexing ligands. In addition, the Pt was deposited onto Ru through bridged-oxygen instead of forming a direct Pt-Ru bonding during displacement reaction.

## Acknowledgements

In the beginning, it is a great honor to express my deepest gratitude to two of my dedicated advisors, Prof. Pu-Wei Wu and Dr. Jyh-Fu Lee, for their superior guidance so that this thesis could have been completed. They have given me a lot of advice, inspirations, solutions, and criticisms with their profound knowledge in science and research experiences. I sincerely appreciate their patience and kindness, because they always put high priority on my experiments and thesis writing. Besides, they spend precious hours to discuss with me anytime they are available. I have learnt from them a lot not only about conducting scientific research, but also professional ethics. This thesis would not have been possible unless the guidance given by my two advisors.

In addition, I am grateful to the senior graduate student, Robert Hsieh, who taught me in establishing all practices and experimental set ups related to the research topic. Ideas and comprehension related to the research were formed after many enthusiastic discussions and brainstorming with him. He has made available his support in a number of ways and I would like to thank Robert for all his help.

Special thanks are also given to senior Ph.D students, Jeff Chang, Kiokio Hsieh, Lawrence Lin, Rebecca Chen, Eric Chang, and Eric Hwang, for their consultations and encouragements. Moreover, I am indebted to many of my colleagues, Tiffany Chiu, Hedy Wang, Joyce Chen, Wayne Chen, Edward Chang, Martin Liao, Tim Hwang, Fiona Chen, Feon Chen, Lisa Chou, and Lynn Hwang for their friendship and support.

I wish to extend my thanks to the staff of department office, Debbie Fu, for her support for paper works. Thanks are also due to my friend, Evelyn Sung, for every touching moments and caring advice when I was troubled. I owe many thanks to my roommates, Brian Ho and Patrick Lee, for being nice and considerate.

At last but not the least, I would like to express my gratitude to my parents and younger sister for taking care of me and supporting me along the way of my study.

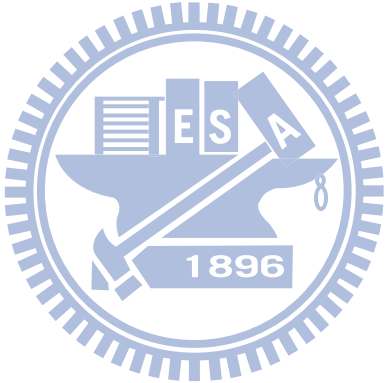
# Table of Contents

|   |      |
|---|------|
| Chinese Abstract .....                                    | i    |
| English Abstract.....                                     | iii  |
| Acknowledgements.....                                     | iv   |
| Table of Contents.....                                    | v    |
| List of Tables .....                                      | vii  |
| List of Figures.....                                      | viii |
| Chapter 1 Introduction .....                              | 1    |
| 1.1 Background .....                                      | 1    |
| 1.2 Motivation .....                                      | 2    |
| Chapter 2 Literature Review .....                         | 5    |
| 2.1 Anode catalysts for DMFC.....                         | 5    |
| 2.2 Platinum monolayer fuel cell electro-catalyst.....    | 8    |
| 2.3 X-ray Absorption Spectroscopy of DMFC Catalysts.....  | 11   |
| Chapter 3 Experimental.....                               | 15   |
| 3.1 Functionalization of commercial carbon XC-72R .....   | 15   |
| 3.2 Fabrication of carbon supported Ru nanoparticles..... | 15   |
| 3.3 Samples for displacement reaction.....                | 15   |
| 3.4 XRD, TEM, EDX and ICP-MS measurements.....            | 16   |
| 3.5 XAS measurements .....                                | 16   |
| 3.6 EXAFS data analysis .....                             | 17   |
| Chapter 4 Results and discussion.....                     | 19   |
| 4.1 Introduction.....                                     | 19   |
| 4.2 Results and discussion .....                          | 20   |



Chapter 5 Conclusions ..... 47

Reference ..... 47



## List of Tables

|  |    |
|--|----|
| Table 1. Results from material characterizations on group A, the immersion baths of group A and the immersion baths of reference group by ICP-MS. .... | 25 |
| Table 2 Results from material characterizations on Ru/C immersed with pH 1, pH 2.2 and pH 8 H <sub>2</sub> PtCl <sub>6</sub> (group A) by EDX. ....    | 26 |
| Table 3 The fitting results from the analysis of Ru K-edge EXAFS spectra. ....   | 37 |
| Table 4 The fitting results from the analysis of Pt L <sub>3</sub> -edge EXAFS spectra. ....   | 45 |



## List of Figures

|   |    |
|---|----|
| Figure 1. The synthesis methods for carbon supported PtRu catalysts: (1) impregnation method, (2) colloidal method, and (3) microemulsion method [6]..... | 7  |
| Figure 2. A sub-monolayer Pt on Ru nanoparticles [19]. .....  | 10 |
| Figure 3. A model of fabricating monolayer Pt on palladium nanoparticles with Cu UPD [19]. .....  | 10 |
| Figure 4. The cyclic voltammetric (CV) scans of new class catalyst and commercial PtRu for MOR [19].....  | 10 |
| Figure 5. The CV scans of Au modified Pt/C [19] .....   | 11 |
| Figure 6. XAS spectrum of Mo K-edge [25].....   | 13 |
| Figure 7. The experimental set up for XAS analysis. (a) Transmission mode; (b) fluorescence mode [25]. .....  | 14 |
| Figure 6(A). The XRD patterns for carbon supported Ru (Ru/C), group A pH 1, pH 2.2, pH 8 and pure carbon. ....  | 22 |
| Figure 6(B). The XRD patterns at 38 degrees for group A pH 1, pH 2.2, and pH 8. ....  | 22 |
| Figure 7(A). The XRD patterns for carbon supported Ru (Ru/C), group B pH 1, pH 2.2, pH 8 and 23   |    |
| Figure 7(B). The XRD patterns at 38 degrees for group B pH 1, pH 2.2, and pH 8. ....  | 23 |
| Figure 8(A). The XRD patterns for carbon supported Ru (Ru/C), group C pH 1, pH 2.2, pH 8 and 24   |    |
| Figure 8(B). The XRD patterns at 38 degrees for group C pH 1, pH 2.2, and pH 8. ....  | 24 |
| Figure 9. The TEM images for carbon supported Ru. ....  | 27 |
| Figure 10. The TEM images for group A, Ru/C immersed with pH 1 H <sub>2</sub> PtCl <sub>6</sub> . ....  | 28 |
| Figure 11. The TEM images for group B, Ru/C immersed with pH 2.2 H <sub>2</sub> PtCl <sub>6</sub> . ....  | 29 |

|  |    |
|--|----|
| Figure 12. The TEM images for group C, Ru/C immersed with pH 8 H <sub>2</sub> PtCl <sub>6</sub> .  | 30 |
| Figure 13. Ru K-edge XANES spectra of Ru metallic powder, RuO <sub>2</sub> , Ru/C immersed with HClO <sub>4</sub> , DI water and KOH.  | 32 |
| Figure 14. Ru K-edge XANES spectra of Ru metallic powder, RuO <sub>2</sub> , Ru/C immersed with pH 1, pH 2.2 and pH 8 H <sub>2</sub> PtCl <sub>6</sub> (group A).                                    | 32 |
| Figure 15. Ru K-edge XANES spectra of Ru metallic powder, RuO <sub>2</sub> , hydrogen reduced Ru/C immersed with pH 1, pH 2.2 and pH 8 H <sub>2</sub> PtCl <sub>6</sub> (group B).                   | 33 |
| Figure 16. Ru K-edge XANES spectra of Ru metallic powder, RuO <sub>2</sub> , Ru/C immersed with pH 1, pH 2.2 and pH 8 H <sub>2</sub> PtCl <sub>6</sub> and followed by hydrogen reduction (group C). | 33 |
| Figure 17. Ru K-edge EXAFS spectra of Ru/C immersed with HClO <sub>4</sub> , DI water and KOH.   | 35 |
| Figure 18. Ru K-edge EXAFS spectra of Ru/C immersed with pH 1, pH 2.2 and pH 8 H <sub>2</sub> PtCl <sub>6</sub> (group A).   | 35 |
| Figure 19. Ru K-edge EXAFS spectra of hydrogen reduced Ru/C immersed with pH 1, pH 2.2 and pH 8 H <sub>2</sub> PtCl <sub>6</sub> (group B).  | 36 |
| Figure 20. Ru K-edge EXAFS spectra of Ru/C immersed with pH 1, pH 2.2 and pH 8 H <sub>2</sub> PtCl <sub>6</sub> and followed by hydrogen reduction (group C).  | 36 |
| Figure 21. Pt L <sub>3</sub> -edge XANES spectra of Pt foil, H <sub>2</sub> PtCl <sub>6</sub> solution adjusted to pH 1, pH 2.2 and pH 8.  | 39 |
| Figure 22. Pt L <sub>3</sub> -edge XANES spectra of Pt foil, Ru/C immersed with pH 1, pH 2.2 and pH 8 H <sub>2</sub> PtCl <sub>6</sub> (group A).  | 40 |
| Figure 23. Pt L <sub>3</sub> -edge XANES spectra of Pt foil, hydrogen reduced Ru/C immersed with pH 1, pH 2.2 and pH 8 H <sub>2</sub> PtCl <sub>6</sub> (group B).                                   | 40 |
| Figure 24. Pt L <sub>3</sub> -edge XANES spectra of Pt foil, Ru/C immersed with pH 1, pH 2.2 and pH 8 H <sub>2</sub> PtCl <sub>6</sub> and followed by hydrogen reduction (group C).                 | 41 |
| Figure 25. Pt L <sub>3</sub> -edge EXAFS spectra of H <sub>2</sub> PtCl <sub>6</sub> solution adjusted to pH 1, pH 2.2 and pH 8.   | 43 |

Figure 26. Pt L<sub>3</sub>-edge EXAFS spectra of Ru/C immersed with pH 1, pH 2.2 and pH 8 H<sub>2</sub>PtCl<sub>6</sub> (group A). ..... 43

Figure 27. Pt L<sub>3</sub>-edge EXAFS spectra of hydrogen reduced Ru/C immersed with pH 1, pH 2.2 and pH 8 H<sub>2</sub>PtCl<sub>6</sub> (group B). ..... 44

Figure 28. Pt L<sub>3</sub>-edge EXAFS spectra of Ru/C immersed with pH 1, pH 2.2 and pH 8 H<sub>2</sub>PtCl<sub>6</sub> and followed by hydrogen reduction (group C). ..... 44



# Chapter 1 Introduction

## 1.1 Background

The Galvanic displacement reaction has received considerable attention and research effort as one of important methodologies to prepare platinum-based anode and cathode catalysts for direct methanol fuel cells (DMFCs), in order to achieve dramatic reduction of precious metal content and improvement of mass activity. Nano-sized catalysts including mono-layers, clusters and alloys are formed based on displacement reaction, because the replacement of non-noble metals by noble metals provides the manipulation of surface atomic morphology.

Similar phenomena observed by Adzic et al and were described as spontaneous deposition or irreversible adsorption. Platinum ions were reduced to metallic state onto ruthenium nanoparticles accompany with the dissolution of ruthenium. However, detailed reaction mechanism such as byproducts, oxidation states and effects caused by various pH values still requires further investigation. A thorough study by Manandhar et al reported for the first time that XPS data shows partially reduced platinum to intermediate oxidation state between solvated species and that of metal, after spontaneously deposited onto ruthenium single crystal without any externally applied potential. For platinum spontaneous deposition at various pH values, clarifications only indicated that platinum complex was adsorbed at the substrate surface with certain oxidation states.

In this research, in-situ X-ray Absorption Spectroscopy is performed to observe the reaction process of displacement reaction. Ruthenium nanoparticles are immersed into hexachloroplatinic acid under various pH conditions. For the platinum precursor, hexachloroplatinic acid, used in this research, a fundamental investigation was performed by Spieker et al. Platinum complex has various forms to maintain stability influenced by pH value, platinum concentration and chloride concentration. Clarifications to oxidation states change and neighboring species of platinum and

ruthenium atoms during the reaction process can be provided based on XANES and EXAFS analysis. Furthermore, two mechanisms including either replacement between platinum and ruthenium atoms or spontaneous deposition of platinum atoms accompany with the oxidation of ruthenium will be justified.

## 1.2 Motivation

The existence of human beings has been lasting for almost two hundred thousand year and increasing. Highly developed society shows that the progress of civilization has prospered exponentially regarding the field of all kinds. However, the nature that keeps all living creatures alive unfortunately reveals the opposite consequences based on the symptoms including the green house effect, pollution, ozone depletion, and energy crisis. One of the important issues that affect instantaneously to all people on Earth is the energy crisis. Precautionary measures have taken with the best of research facilities, governments, and even individuals in order to eliminate the impact brought by the exhaustion of energy. A majority of energy source originates from fossil fuel. The forecast of depleting fossil fuel has emphasized based on its dramatic consumption. The development of alternative energy has received people's attention considerably for the sake that usable energy still exists on the moment when all fossil fuel reaches its end. The fuel cell is one of the promising solutions that provide reliable and clean energy source. Many different kinds of fuel cells such as Polymer Electrolyte Membrane Fuel Cells, Alkaline Fuel Cells, Phosphoric Acid Fuel Cells, Molten Carbonate Fuel Cells, and Solid Oxide Fuel Cells have been developed with the progress of human technologies. A great amount of research is focused on Polymer Electrolyte Membrane Fuel Cells (DMFC) due to its outstanding properties including high energy density, portability, low working temperature, etc.

The performance of DMFC relies greatly on its catalysts on the anode for methanol oxidation

reaction (MOR) and cathode for oxygen reduction reaction (ORR). PtRu is a bimetallic compound often used as anode catalyst due to its catalytic activity for MOR and outstanding CO-resistance. For cathode materials, Pt-based and non Pt-based materials have been thoroughly investigated elsewhere which are not covered in this study. However, noble metals are major components of catalysts. Because of the cost and rarity, the reduction of noble metal loading and enhancement of catalysis efficiency have become essential issues throughout the research topics. Significant reduction of noble metal loading is widely proposed as a crucial methodology to achieve improvements on electrochemical active materials. Obstacles were found for dramatic reduction the noble metal loading and further improvement the catalytic MOR activity in the meanwhile. In the recent research by Adzic et al., monolayer-level Pt was synthesized with galvanic displacement reaction, which provides enhanced mass activity and durability for MOR compared with commercial carbon supported PtRu.

The fabrication method involved with galvanic displacement reaction for Pt and Ru atoms somehow suffer from its opaque mechanism. Possibilities of chemical reactions happening on the Ru surface consist of either the oxidation of Ru to Ru(OH), or a higher oxidation state of Ru, or any other probable reactions. On the other hand, the possible dissolution of Ru, which also contributes the displacement reaction, should be taken into consideration. The acidic aqueous environment in which the displacement reaction occurs is feasible to dissolve Ru. The dissolved Ru and displaced Ru are substantially mixed together and both results are received during the analysis. On the other hand, the whole reaction takes place in aqueous phase and solid phase.

Characterizations taken under ultra high vacuum environment lead to the difficulty of objective observations and analysis with instrument as X-ray photoelectron spectroscopy (XPS) and scanning electron microscopy/energy disperse spectrometer (SEM/EDS). X-ray absorption spectroscopy (XAS) has increasingly received attention for its appropriate analytical instrument for PtRu bimetallic alloys. XAS contributes the unique information regarding the oxidation state,



coordination environment, coordination number and bond lengths of the absorbing atom. Remarkably, in-situ measurement can be conducted which is close to working condition of as-observed specimens.

The investigation of galvanic displacement reaction mechanism is attempted in this work with XAS and other analytical instrument. Based on the information of the reaction mechanism, the optimized fabrication process for catalysts involving Pt and Ru atoms should be accomplished.



## Chapter 2 Literature Review

### 2.1 Anode catalysts for DMFC

Over the decades, researchers have been eagerly searching for alternative energy sources for solving the energy crisis. The urgent need originates from high-energy demands, fossil fuel depletion, environmental pollution, etc. Among many technologies under development, fuel cells have become one of the candidates that provide an efficient and clean energy source. There are various sorts of fuel cells. In particular, a promising type known as direct methanol fuel cell (DMFC) has received considerable attention due to its favorable characteristics with respect to fuel usage and feed strategies [1-2].

It is well known that the key materials that greatly affect the performance of a DMFC are the membrane and electro-catalyst. Unfortunately, severe challenges are present for the electro-catalyst such as the mass activity, reliability, durability, and cost reduction. The improvement of anode catalyst for methanol oxidation reaction (MOR) has been accomplished with the exploration of noble and non-noble electrochemical active materials. Compared with non-noble catalysts, noble metal catalysts such as Pt, demonstrates reasonable electrochemical activity and stability. For the objective of cost reduction and performance improvement, the strategy has shifted to identifying alloys with comparable performance. To date, PtRu alloys have emerged as the leading material that seem to be the state-of-the-art binary anode catalyst.

Pure Pt atom goes through a series of reactions for MOR [3], including (1) methanol adsorption; (2) C-H bond activation (methanol dissociation); (3) water adsorption; (4) water activation; and (5) CO oxidation. Though out the reaction process, high potential is required to form OH by activating water on the Pt surface which is necessary for the oxidative removal of adsorbed CO. If not, the CO is considered to be a poisoning substance among the intermediates in MOR that occupy the active sites of Pt. However, undesirable high potential limits the performance of Pt for

MOR. Therefore, the introduction of complementary metal which provides the oxidative removal of adsorbed CO at lower potential becomes necessary and which leads to the development of Pt-based alloys. To date, PtRu was found to be the outstanding binary alloy among PtOs, PtSn, PtW, PtMo, etc. The enhancement of PtRu catalyst compared with pure Pt for MOR can be attributed to both bi-functional mechanism [4] and ligand effect [5]. Ru induces influences in the electronic structure of Pt which weakens the Pt–CO bond [5]. The bi-functional mechanism implies that the oxygen containing species are adsorbed on the Ru atoms at a lower potential. Therefore, the mechanism of oxidative removal of CO to CO<sub>2</sub> is summarized below [4]:



The catalytic activity of PtRu is greatly influenced by the composition, atomic structure, the degree of alloying, morphology, and particle size. Also, the fabrication methods for PtRu catalysts show specific manipulation of the properties based on the characteristics of each method. There are three principal methods for preparing carbon supported PtRu catalysts. They are impregnation method, the colloidal method, and the microemulsion method. Generally, all methods involve chemical procedures for forming nanoparticles, followed by deposition on the carbon supports with uniform dispersion. The schematic diagram in Figure 1 presents the flow chart for each fabrication methods.

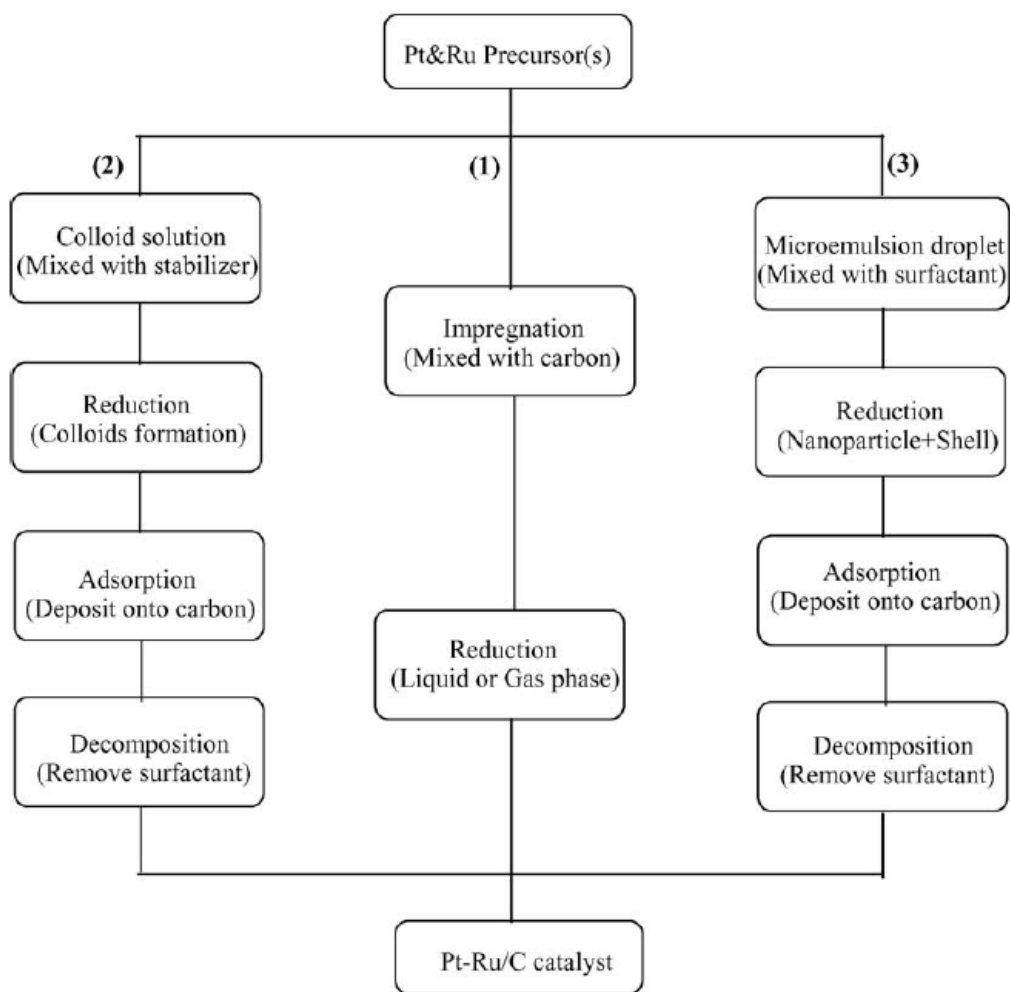


Figure 1. The synthesis methods for carbon supported PtRu catalysts: (1) impregnation method, (2) colloidal method, and (3) microemulsion method [6].

The impregnation method is the most widely used method among the rest due to its simplicity and efficiency [5, 7-8]. First, the Pt and Ru precursors are mixed together with carbon black in aqueous solution for form a homogeneous mixture. Then, the chemical reduction step is carried out by addition of reducing agents such as  $\text{Na}_2\text{S}_2\text{O}_3$ ,  $\text{Na}_4\text{S}_2\text{O}_5$ ,  $\text{NaBH}_4$ ,  $\text{N}_2\text{H}_4$ , or formic acid in solution. Alternatively, the reduction process can be conducted with hydrogen at elevated temperature. Synthetic conditions including the nature of the metal precursors, reduction methods, and heating temperature all play important roles in impregnation process [9-11]. The major weakness of

impregnation method is the difficulty of controlling nanoparticle size and distribution. Moreover, particle segregation on the carbon supports is another frequently encountered issue.

The colloidal method is another preparation method for carbon supported PtRu catalyst [12-14]. Common steps are: (1) preparation of PtRu colloids; (2) deposition of such colloids onto the carbon support; (3) and chemical reduction of the mixture. For example, a well-established colloidal method was proposed by Watanabe et al. in which co-deposition of colloidal Pt and Ru oxides on carbon in aqueous media was conducted, followed by a reduction with bubbling hydrogen [15]. The metal oxide colloid route offers better specific surface area of PtRu compared with that of conventional impregnation method. However, the control over particle growth and agglomeration are regarded as the weakness of this method.

The microemulsion method is a relatively new route compared with previous ones [16-18]. In this method, the PtRu nanoparticles are formed through a water-in-oil microemulsion reaction, followed by a reduction step. The microemulsion is a nano grade droplet of aqueous noble metal precursor. The droplets are capsuled by surfactant molecules and dispersed uniformly in an immiscible organic solvent. The reduction step can be performed by adding a reducing agent into the microemulsion system or mixing it with another microemulsion system containing suitable reducing agents. Therefore, the reduction reaction is confined in the nano-grade droplet, so that the particle size can be easily controlled by the magnitude of the microemulsion size. The surfactant around the droplet serves as a protection from the agglomeration of PtRu nanoparticles. The removal of the surfactant molecules can be achieved by proper heat treatment. The main advantage of microemulsion method is the ease to control metallic composition and particle size within a narrow distribution by optimized fabrication conditions.

## 2.2 Platinum monolayer fuel cell electro-catalyst

A new class of electro-catalyst was proposed by Adzic et al. for MOR and oxygen reduction reaction (ORR). Its notable advantages consist of high Pt utilization, enhanced activity, and stability, and direct correlations between catalytic activities and physical properties [19]. This new class of electro-catalyst is composed of Pt monolayer on carbon supported metal or metal alloy nanoparticles. With this unique metal catalyst structure, the problems of conventional catalyst of high Pt loading and low efficiency can be largely resolved. The applications of such catalyst were demonstrated with sub-monolayer Pt on Ru nanoparticles for hydrogen oxidation reaction (HOR) [20], and monolayer Pt on palladium nanoparticles for the ORR [21-23].

Fabrication methods for depositing Pt sub-monolayers on Ru and of Pt mixed Pt-based monolayers on noble metal substrates are mainly based on the electroless (spontaneous) deposition of Pt on Ru. Preparation of sub-monolayer Pt on Ru nanoparticles involves heating carbon supported Ru in a hydrogen atmosphere at 300 °C to reduce the surface RuOH. Afterwards, the samples are immersed in hexachloroplatinic acid. The entire process is carried out in argon atmosphere [24]. To prepare monolayer Pt on palladium nanoparticles entails a Cu monolayer deposited at underpotentials (UPD) and the Cu is galvanically displaced after the immersion of  $K_2PtCl_4$  solution. The as-prepared catalysts from these two approaches are schematically exhibited in Figure 2 and 3. The electrochemical mass activity of sub-monolayer Pt is shown in Figure 4.

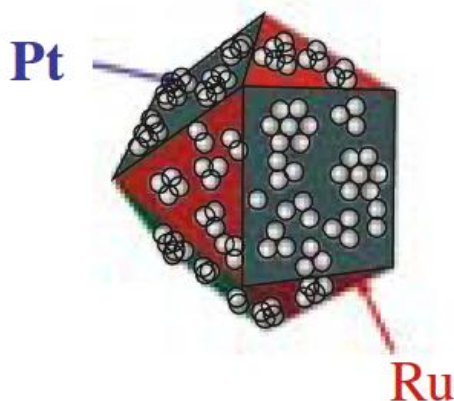


Figure 2. A sub-monolayer Pt on Ru nanoparticles [19].

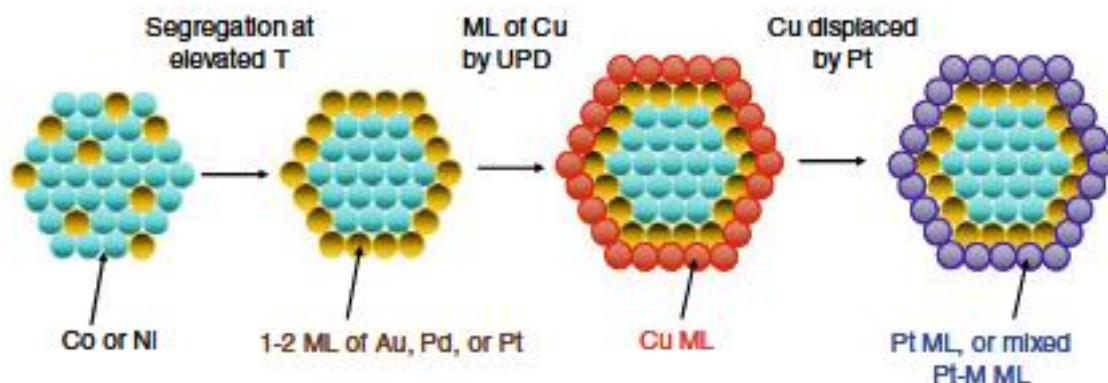


Figure 3. A model of fabricating monolayer Pt on palladium nanoparticles with Cu UPD [19].

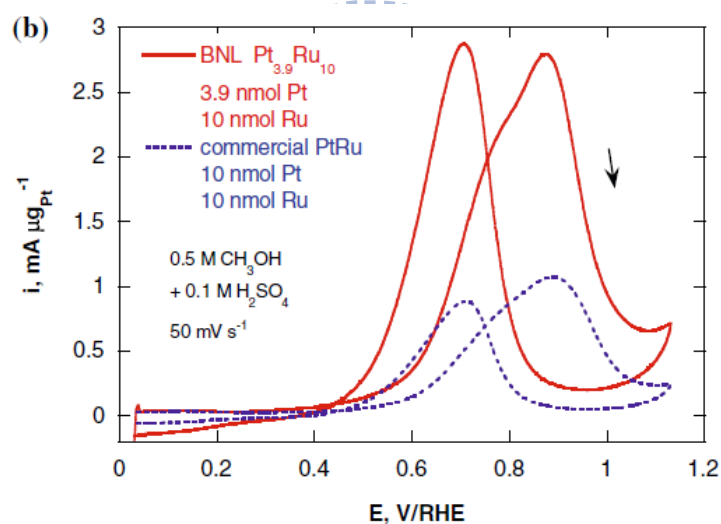


Figure 4. The cyclic voltammetric (CV) scans of new class catalyst and commercial PtRu for MOR [19]

The fabrication method for this new class catalyst, the displacement reaction, can also be applied to depositing additional gold cluster for the purpose of durability enhancement of the Pt catalyst. That is, the Au modified Pt shows notable prevention from Pt dissolution and excellent stability during potential cycling. In Figure 5, the electrochemical surface area of Au modified Pt

displays negligible after the potential cycling.

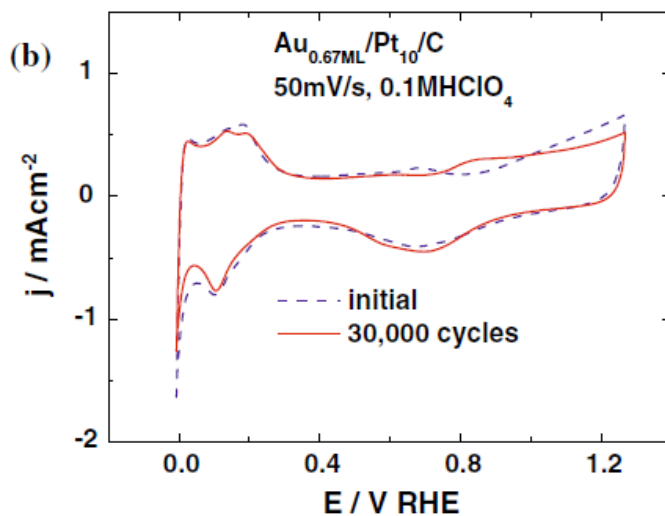


Figure 5. The CV scans of Au modified Pt/C [19]

### 2.3 X-ray Absorption Spectroscopy of DMFC Catalysts

X-ray absorption spectroscopy (XAS) has been employed as an useful tool to launch the scientific research on fuel cell catalysts for the last two decades [25]. The advantages of performing research with XAS is that multiple information can be acquired regarding the oxidation states, local coordination, numbers and identities of neighboring atoms of the absorbing atom. Moreover, the ability to conduct in situ analysis, in the environments that is similar to the working condition is irreplaceable other than the instrument requiring an ultra high vacuum environment.

An XAS measurement is to detect the changes of the absorbance or the fluorescence of the sample while it is scanned by X-ray with energy below the absorption edge to above that. Figure 6 is a typical XAS spectrum. The absorption,  $\mu_x$ , is defined by the Beer Lambert equation,

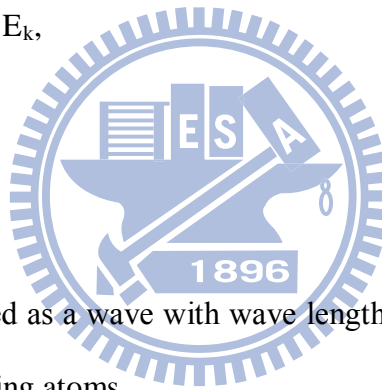
$$\mu_x = \log (I_0/I_t) \quad (1)$$



where  $\mu$  is the linear absorption coefficient,  $x$  is the sample thickness,  $I_0$  is the intensity of the incident X-ray, and  $I_t$  is the transmitted X-ray. X-ray absorption near edge structure (XANES) is the region close to the absorption edge that results from the excitation of the core level electron to unoccupied orbital by the sufficient X-ray photon. XANES is related to the local symmetry and electronic structure of the absorbing atom. The absorption edge can provide the information about the oxidation states of the sample, the absorbing element. The XANES region extends to around 50 eV above the absorption edge [25-26].

At higher incident X-ray energy approximately 50 eV to 1000 eV above the absorption edge, the energy of photons is sufficient to excite the core level electron into the continuum, producing a photoelectron with kinetic energy,  $E_k$ ,

$$E_k = h\nu - E_{\text{binding}}$$



(2)

The excited electron can be seemed as a wave with wave length  $\lambda$  given by the de Broglie relation, which is scattered by the neighboring atoms.

$$\lambda = h / p$$

(3)

The interference between the outgoing wave and backscattered wave contributes the oscillation in the absorbance as a function of the energy of the incident X-ray. These oscillations are called the extended X-ray absorption fine structure (EXAFS). Due to the contribution of the EXAFS originates from the neighbor atoms of the absorbing atom, the analysis of the EXAFS provides the information regarding the identity, distance and the number of neighboring atoms [25-26].

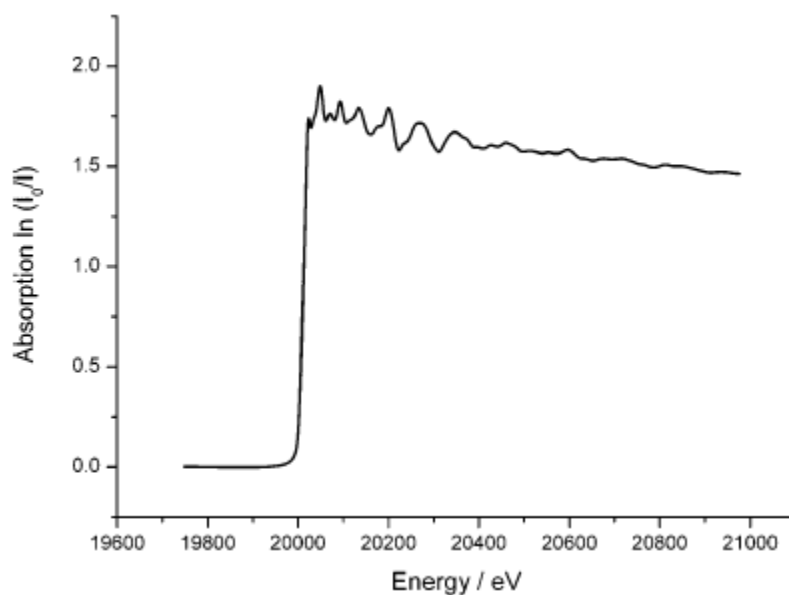


Figure 6. XAS spectrum of Mo K-edge [25]

The XAS experiments require an intense and continuous radiation light source. Usually, the measurement takes place with synchrotron radiation facilities. Figure 7 shows the experimental set up of XAS analysis. Generally, transmission mode is used to collect XAS data. However, fluorescence mode becomes more appropriate when measuring dilute samples. The intensity of the X-ray is monitored before and after penetrating the sample, defined as  $I_0$  and  $I_t$  ( $I_f$ ), respectively. Ionization chamber detectors are applied to detect the photon intensity, except Lytle detector is for fluorescence intensity.

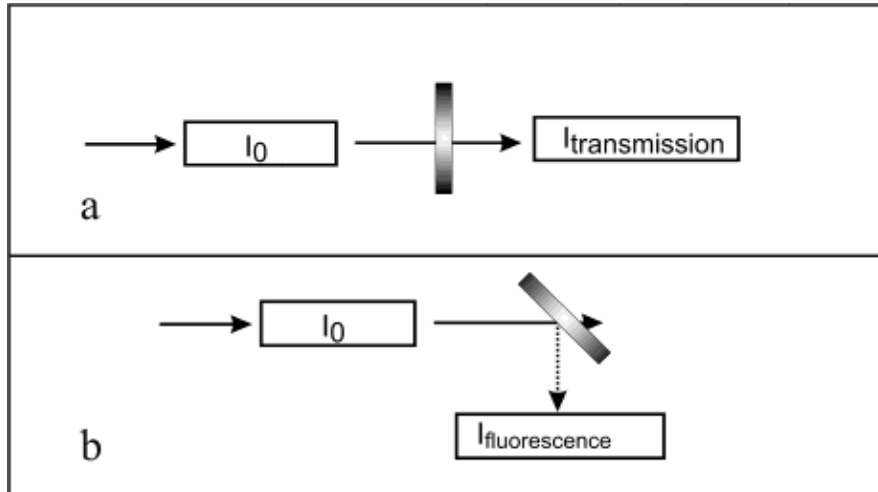
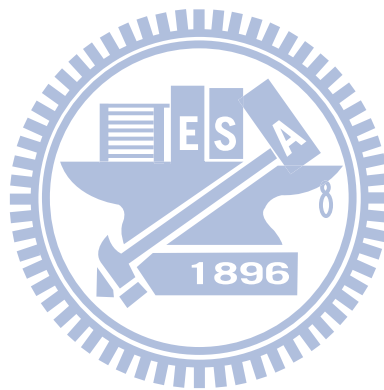


Figure 7. The experimental set up for XAS analysis. (a) Transmission mode; (b) fluorescence mode

[25].



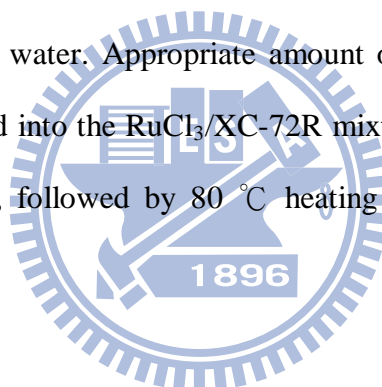
## Chapter 3 Experimental

### 3.1 Functionalization of commercial carbon XC-72R

Functionalization of commercial carbon XC-72R was conducted by immersing XC-72R into pure sulfuric acid (97 wt%) and nitric acid (61 wt%) at 3:1 volume ratio for 1 h at 25 °C. The pretreatment was imposed to increase the adhesion of chemically reduced Ru nanoparticles by providing suitable functional groups on the carbon support [39].

### 3.2 Fabrication of carbon supported Ru nanoparticles

Ru nanoparticles were deposited onto functionalized commercial carbon XC-72R via a chemical reduction method. Mixture 0.2 g of RuCl<sub>3</sub> and 0.8 g of functionalized XC-72R were dissolved in excess of de-ionized water. Appropriate amount of NaBH<sub>4</sub> was then dissolved with de-ionized water and slowly added into the RuCl<sub>3</sub>/XC-72R mixture. Then, the mixture was filtered and washed by de-ionized water, followed by 80 °C heating in oven to remove the remaining solvent.



### 3.3 Samples for displacement reaction

The carbon supported Ru nanoparticles were deposited on a 2 × 2 cm<sup>2</sup> carbon cloth (E-TEK) by an ink method. The ink was composed of 8 mg carbon supported Ru nanoparticles, 5 mg PTFE (30 wt%) and 5 mL 99.5 wt% ethanol, the ink was well-dispersed by supersonication for 30 minutes. Subsequently, the ink dispersion was drop-wisely deposited on a 2 × 2 cm<sup>2</sup> carbon cloth which was kept atop a hot plate at 80 °C. After the residual solvent was dried, the Ru/C coated carbon clothes were immersed into 5 mM intrinsic hexachloroplatinic acid aqueous solution with three different pH values (1.0, 2.2 and 8.0). The nature for 5 mM hexachloroplatinic acid was pH 2.2, and the pH value was adjusted to pH1 by perchloric acid and pH 8 by potassium hydroxide, respectively. The immersion lasted for 24 hours at 40 °C. The as-prepared samples were thoroughly rinsed with

de-ionized water, noted as group A. The second identical set of samples was fabricated, defined as group B, with the same fabrication process except the Ru/C was subjected to hydrogen reduction before the immersion in hexachloroplatinic acid solution. The third set of samples undergoing a hydrogen reduction after the immersion in hexachloroplatinic acid solution was labeled as group C. The hydrogen reduction was conducted with pure hydrogen under 1 atm at 80 °C for two hr. For samples in reference groups, the immersion baths were replaced by perchloric acid (pH 1), potassium hydroxide (pH 8) and de-ionized water, respectively.

### 3.4 XRD, TEM, EDX and ICP-MS measurements

X-ray diffraction (XRD) patterns for the as-prepared samples were obtained by Max Science-M18XHF KXY-8019-1 with a Cu K $\alpha$  source of 1.54 Å. The X-ray diffractogram was received at a scan speed of 4 degrees/second for 2 $\theta$  values between 30° and 90°. Transmission Electron Microscopy (TEM) was performed to observe the morphology of the as-prepared nanoparticles using JEOL JEM-3000F with an accelerating voltage of 300 kV. Approximate element composition was acquired with energy-dispersive X-ray spectroscopy (EDX) equipped on the TEM. The exact metal loadings were determined by an inductively coupled plasma mass spectrometry (ICP-MS).

### 3.5 XAS measurements

X-ray absorption spectra (XAS) for Pt L<sub>3</sub>-edge (11,564 eV) and Ru K-edge (22,117 eV) were obtained at end stations BL01C1 and BL17C1 of the Taiwan Light Source (TLS), National Synchrotron Radiation Research Center (NSRRC), Hsinchu, Taiwan. The storage ring energy was 1.5 GeV, and the stored top-up ring current was in the range of 300-360 mA. A double Si(111) crystal monochromator was employed for energy selection with a resolution  $\Delta E/E$  better than  $2 \times 10^{-4}$  at both end stations. Rh or Pt-coated mirrors were adopted to reject high-order harmonics,

collimate (upstream) and refocus (downstream). The XAS measurements were carried out in fluorescence mode of detection at 25 °C. A Lytle fluorescence detector along with three gas-filled ionization chambers were used to collect the intensities of the X-ray fluorescence photons from an as-prepared sample ( $I_f$ ), the incident beam ( $I_0$ ), the transmitted beam through the sample ( $I_t$ ), and the transmitted beam through reference metal foil or powder ( $I_r$ ). A Pt foil was served as reference for Pt  $L_3$ -edge measurements and Ru powder was served as that for Ru K-edge measurements.

### 3.6 EXAFS data analysis

Extended X-ray absorption fine structure (EXAFS) data analysis and fitting were processed by IFEFFIT 1.2.11c data analysis package (Athena, Artemis, and FEFF6) [14-15]. The raw data were calibrated by aligning the scans against the reference and merging multiple scans as an average to achieve better signal quality. X-ray absorption near edge structure (XANES) spectra were obtained after appropriate process by Athena software. The EXAFS function was obtained by standard procedures with Athena including pre-edge and post-edge background subtractions, and normalization with respect to the edge jump. The detailed procedure has been reported elsewhere [16]. The resultant EXAFS function,  $\chi(E)$ , was then transformed from energy space to k-space. The value k refers to photoelectron wave vector. At the high k-region of  $\chi(k)$  data, multiplication by  $k^3$  was conducted to compensate the damping of EXAFS oscillations. Next,  $k^3$  weighted  $\chi(k)$  data were Fourier transformed to r-space. Specific ranges in k-space for the Fourier transformation were selected from 3.32 to 12.74  $\text{\AA}^{-1}$  for the Pt  $L_3$ -edge and 4.01 to 13.42  $\text{\AA}^{-1}$  for the Ru K-edge. The EXAFS curve fitting in r-space was applied by a nonlinear least-square algorithm. Also, the r-space ranges for the curve fitting were established from 1.29 to 3.12  $\text{\AA}$  (without phase correction) for Pt and 1.32 to 2.73  $\text{\AA}$  for Ru. The structural parameters were fitted by Artemis with the theoretical standards generated by FEFF6 code [17]. The fitted structural parameters include the coordination number (N), bond distance (R), Debye–Waller factor ( $\Delta\sigma_j^2$ ), and inner potential shift ( $\Delta E_0$ ). Two

assumptions were added in the EXAFS fitting for hexachloroplatinic acids. First, we assumed that the Pt ion (IV) complexes were octahedrally coordinated, which suggested that the sum of Pt-Cl and Pt-O coordination numbers were kept at six for all complexes. Second, the Debye-Waller factor differences of Pt-Cl and Pt-O were assumed to be identical [12]. The amplitude reduction factor ( $S_0^2$ ) for Ru were obtained by analyzing Ru powder and found to be 0.79.



## Chapter 4 Results and discussion

### 4.1 Introduction

PtRu is an anode catalyst for methanol oxidation reaction (MOR). It is known that Ru substantially promotes the CO-resistance of Pt during MOR process. To date, both bifunctional mechanism and ligand effect are proposed to explain the behavior that Ru prevents Pt from CO-poisoning [27-29]. Since both Pt and Ru are precious metals, it becomes an issue of reducing their loading while maintaining necessary catalytic activity. To achieve this objective, a core-shell structure has been explored recently. Of many routes to prepare core-shell structure, the displacement reaction is a novel preparation technique that allows the fabrication of noble metal for electrochemical active materials with ultra low content of Ru or Pt [30-32].

Earlier, fundamental studies related to the displacement reaction conducted by Adzic et al. suggest that the driving force is the potential difference between  $\text{PtCl}_6^{2-}$  reduction and  $\text{Ru}^0$  oxidation [33-35]. However, the detailed mechanism for Pt deposition on Ru still requires further clarification. Possibilities of chemical reactions occurring on the Ru surface consist of either the oxidation of Ru to  $\text{Ru}(\text{OH})$ , or a higher oxidation state of Ru. Alternatively, the possible dissolution of Ru, which also contributes to the displacement reaction, should be taken into consideration. Manandhar et al. emphasized that the spontaneously-deposited Pt on Ru was Pt cations in intermediate oxidation states by X-ray photoelectron spectroscopy (XPS) [36-37]. Pt chloride, oxide, and hydroxide species were observed on Ru substrates depending on various ligand environments of Pt. The oxidation states for the as-deposited Pt were between the state of solvated Pt precursors and that of metallic Pt.

Previous research by Spieker et al. demonstrated that the hexachloroplatinic acid is a strong acid with rapid hydrolysis confirmed by extended X-ray absorption fine structure (EXAFS). A thorough study provides the elucidation regarding the Pt coordination environment for its precursor,



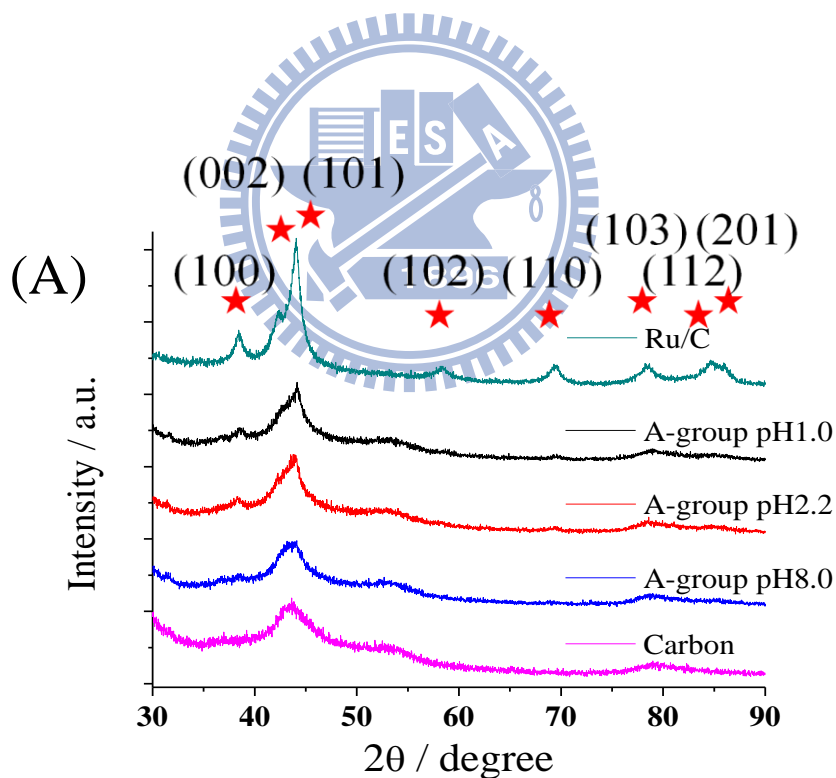
hexachloroplatinic acid, in the form of aqueous solution under various pH values and ion concentrations. The bonding of Pt-oxygen and Pt-chloride play crucial role throughout the reaction of galvanic displacement reaction due to the transition to Pt-Ru bonding. However, a direct and further observation covering from liquid-phased ionic Pt to solid-phased metallic Pt should make a contribution for building up the detailed and complete mechanism. In addition, the acidic aqueous environment in which the displacement reaction occurs is feasible to dissolve Ru. The dissolved Ru and displaced Ru are substantially mixed together and both results are received during the analysis [38].

From the discussion above, a sophisticated analytical method should be developed to provide a further investigation. The Pt deposited with displacement reaction on Ru/C and corresponding liquid phase Pt precursor ought to be taken as correlated analysis to establish the mechanism for PtRu displacement reaction. In this work, X-ray absorption spectroscopy was employed to provide a precise investigation to determine the oxidation states and coordination environment including solid and liquid samples. Inductively coupled plasma mass spectroscopy (ICP-MS) is a quantitative instrument that reveals the exact amount of Pt and Ru atom participating in the displacement process. X-ray diffraction confirms the slight lattice expansion for Pt-deposited Ru compared with pure Ru nanoparticles. Finally, we attempt to establish the detailed reaction involved in the displacement process.

## 4.2 Results and discussion

Figure 6, 7 and 8 demonstrate the XRD patterns for samples from group A, B and C, respectively. The diffraction peaks at the top and bottom of Figure 6(A), 7(A) and 8(A) exhibit patterns for Ru/C, in which the hcp Ru lattice was confirmed, albeit with reduced intensity caused by low loading and interference from carbon support. The diffraction peak at 38.4 degree of Ru (100) phase is selectively shown in Figure 6(B), 7(B) and 8(B) for group A, B and C, respectively.

In Figure 6(B), the diffraction peaks of group A reveal relatively broad compared with the rest groups. In Figure 7(B), peaks are sharpened due to hydrogen reduction and slightly shifted toward lower angles with the sequence of pH 2.2 and pH 1. This indicates that the expansion for the lattice of Ru was caused by the displacement of Pt atoms and their incorporation into Ru lattice. However, the peak position of pH 8 remained the same as pure Ru/C, suggesting that the adsorption of Pt atoms was taking place only on the surface of Ru nanoparticles. In Figure 8(B), diffraction peak at 39.5 degrees for pH 8 was observed that probably was attributed to Pt (111). The presence of Pt diffraction peak suggested that the Pt atoms were present after hydrogen reduction. However, the absence of Pt diffraction peak for pH 1 inferred that the feasibility of forming Pt clusters was reduced due to the incorporation of Pt atoms into Ru lattice, leaving a sub-monolayer Pt on the Ru surface.



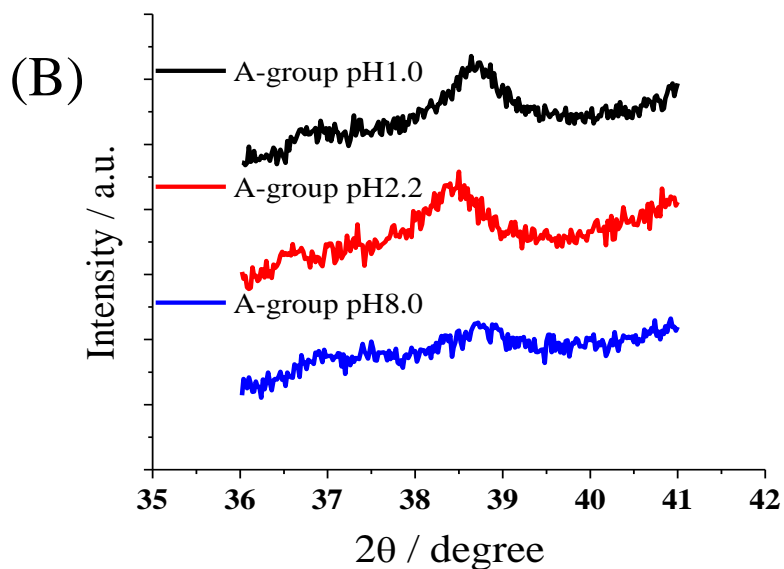
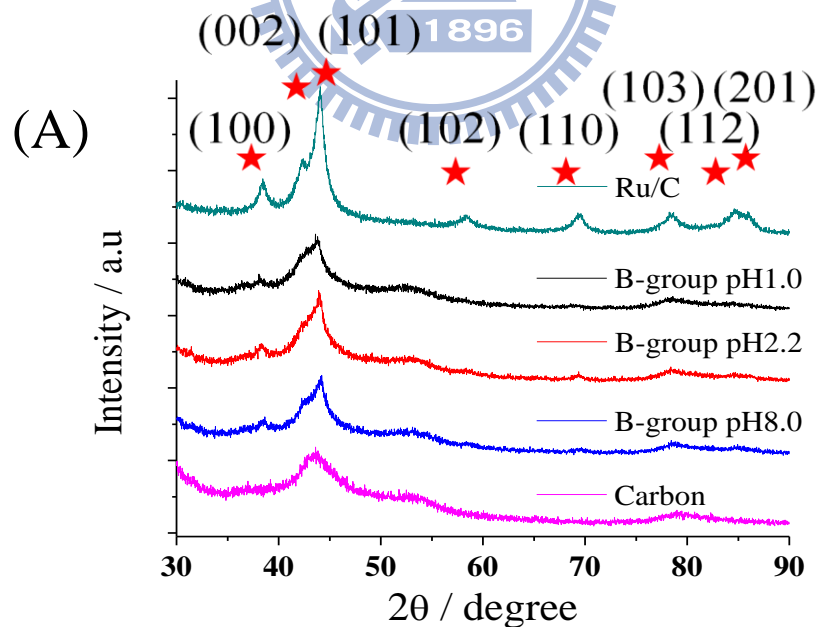


Figure 6(A). The XRD patterns for carbon supported Ru (Ru/C), group A pH 1, pH 2.2, pH 8 and pure carbon.

Figure 6(B). The XRD patterns at 38 degrees for group A pH 1, pH 2.2, and pH 8.



(B)

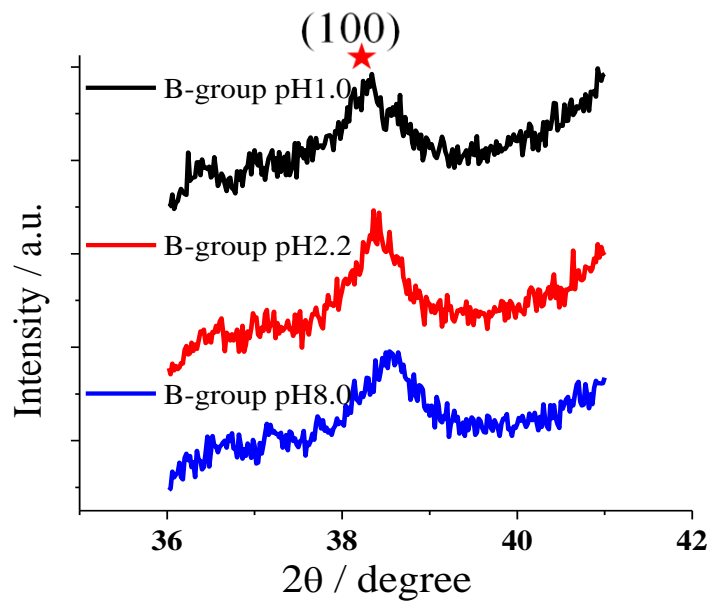
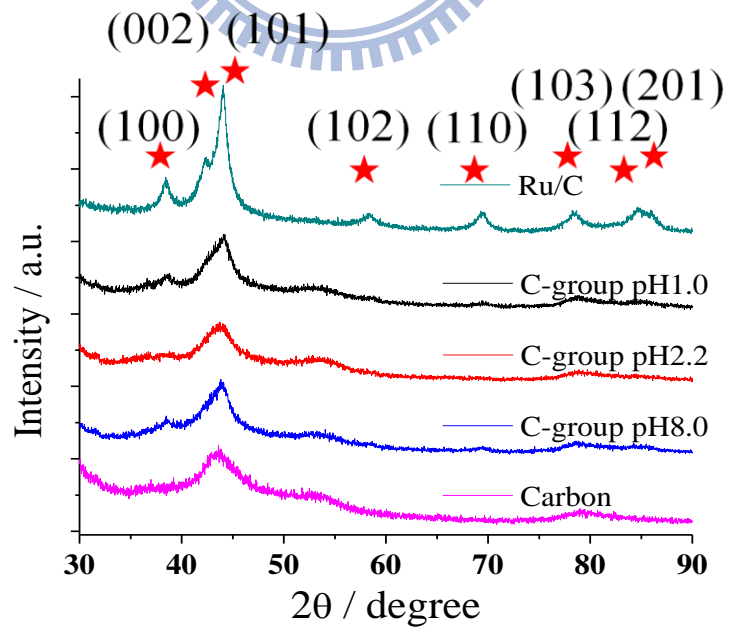


Figure 7(A). The XRD patterns for carbon supported Ru (Ru/C), group B pH 1, pH 2.2, pH 8 and pure carbon.

Figure 7(B). The XRD patterns at 38 degrees for group B pH 1, pH 2.2, and pH 8.



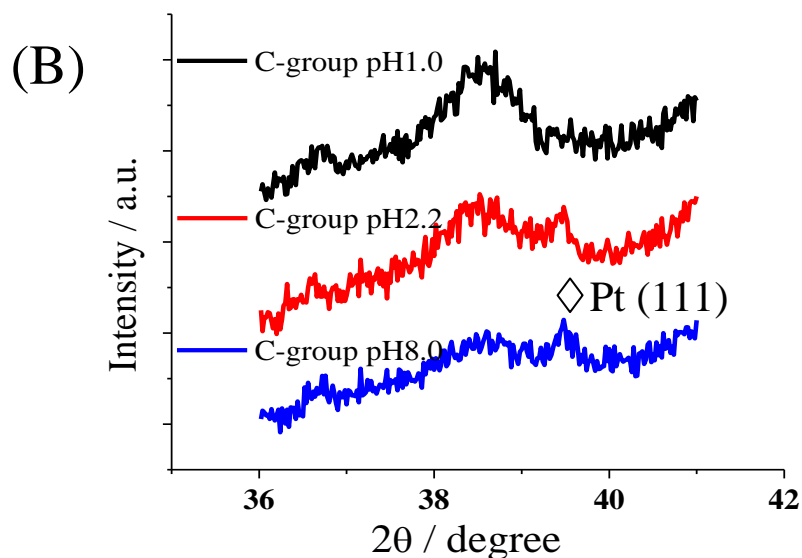


Figure 8(A). The XRD patterns for carbon supported Ru (Ru/C), group C pH 1, pH 2.2, pH 8 and pure carbon.

Figure 8(B). The XRD patterns at 38 degrees for group C pH 1, pH 2.2, and pH 8.

Table 1 presents the ICP-MS results for the as-prepared samples of group A, the corresponding immersion baths of group A, and the immersion baths for reference group. The results indicated Pt loadings were 1.26, 1.17 and 0.62 mmole for pH 1, pH 2.2 and pH 8, respectively. Lower pH value allowed more Pt loading deposited on Ru. On the other hand, the Ru loadings were 2.02, 2.94, and 4.86 mmole for pH 1, pH 2.2 and pH 8, respectively. Apparently, Ru dissolution caused by Pt displacement and acid corrosion was observed. For the corresponding hexachloroplatinic acid immersion baths, the amount of Pt remained around 20 mmole. Generally, more Ru content was detected in the immersion baths of hexachloroplatinic acids rather than that of pure perchloric acid, DI water and potassium hydroxide. These behaviors suggested that a greater amount of Ru atoms was replaced by Pt ions. The dissolution of Ru by acidic or basic solvents still existed but it's

amount was slightly varied.

Table 1. Results from material characterizations on group A, the immersion baths of group A and the immersion baths of reference group by ICP-MS.

|               |   | Pt ( $\mu\text{mole}$ ) | Ru ( $\mu\text{mole}$ ) |
|---------------|---|-------------------------|-------------------------|
| Nanoparticles | pH 1                                    | 1.26                    | 2.02                    |
|               | pH 2.2                                  | 1.17                    | 2.94                    |
|               | pH 8                                    | 0.62                    | 4.86                    |
| Solutions     | H <sub>2</sub> PtCl <sub>6</sub> pH 1   | 20.01                   | 1.88                    |
|               | H <sub>2</sub> PtCl <sub>6</sub> pH 2.2 | 21.61                   | 1.37                    |
|               | H <sub>2</sub> PtCl <sub>6</sub> pH 8   | 22.57                   | 0.05                    |
| Solutions     | HClO <sub>4</sub>                       | N/A                     | 0.31                    |
|               | DI water                                | N/A                     | 0.01                    |
|               | KOH                                     | N/A                     | 0.03                    |

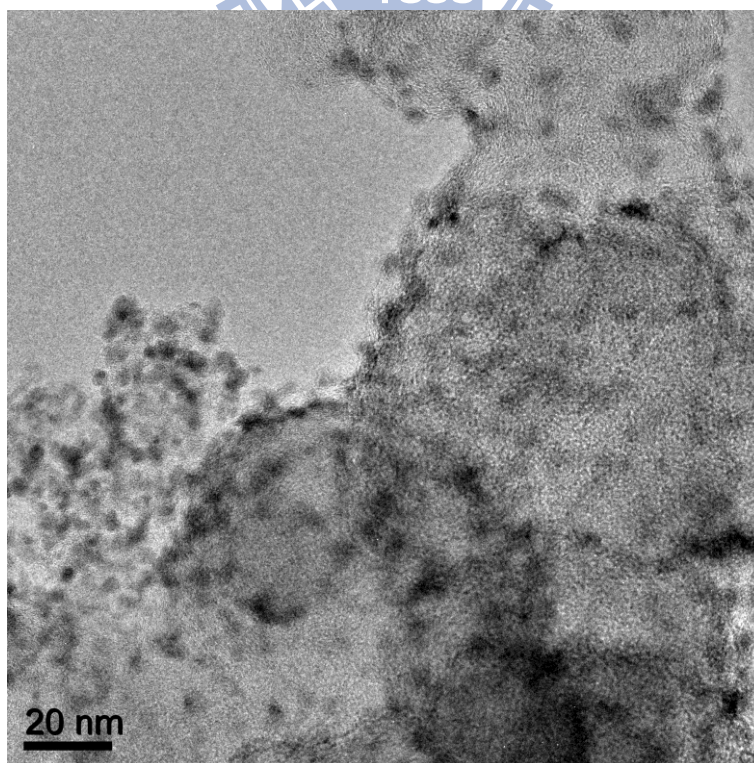
TEM images for carbon supported Ru nanoparticles are exhibited in Figure 9. Ru nanoparticles were well-dispersed with notable size uniformity on the carbon supports. Figure 10 to 12 display the TEM images of group A with various immersion baths of pH 1, pH 2.2 and pH 8. As shown, the PtRu/C particles were uniformly dispersed and their sizes were approximately 2~3 nm. The slight variations of sizes between each groups suggested that the Ru nanoparticles were rather stable in various environments against corrosive dissolution. In addition, possible particle size variation

influenced by acidic immersion or displaced by Pt atoms was negligible. TEM/EDX confirmed the presence of Pt species on the surface of Ru nanoparticles with quantitative results in table 2. The immersion bath of pH 1 possessed a larger amount of deposited Pt relatively compared with that of other pH values. This result suggested that the displacement reaction showed more tendencies to allow the deposition of Pt on Ru nanoparticles in acidic environment than in basic one. The detailed mechanism is explained in the following parts of the discussion.

Table 2 Results from material characterizations on Ru/C immersed with pH 1, pH 2.2 and pH 8

H<sub>2</sub>PtCl<sub>6</sub> (group A) by EDX.

|        | Pt (at%) | Ru (at%) |
|--------|----------|----------|
| pH 1   | 11.08    | 88.92    |
| pH 2.2 | 6.65     | 93.35    |
| pH 8   | 3.38     | 96.62    |





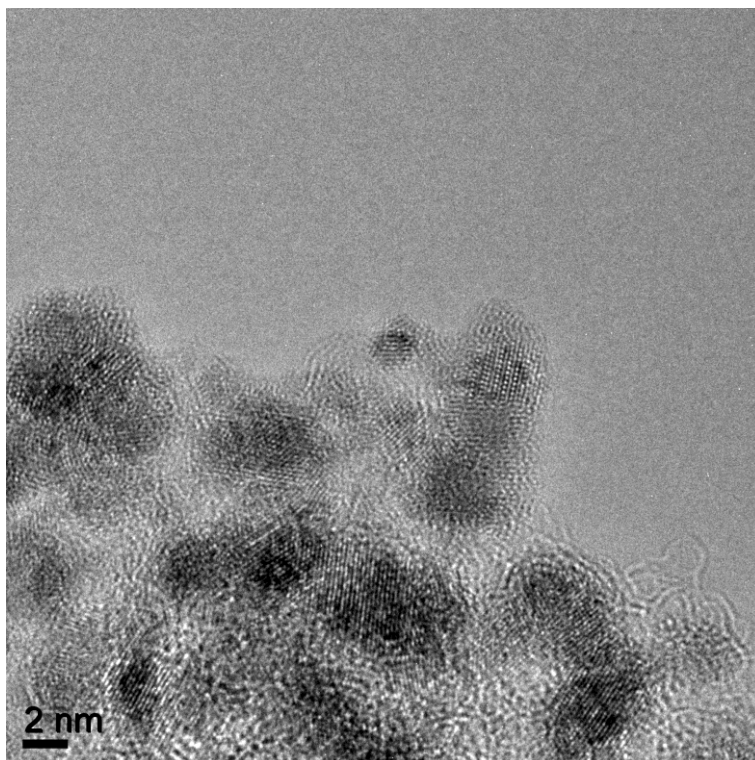
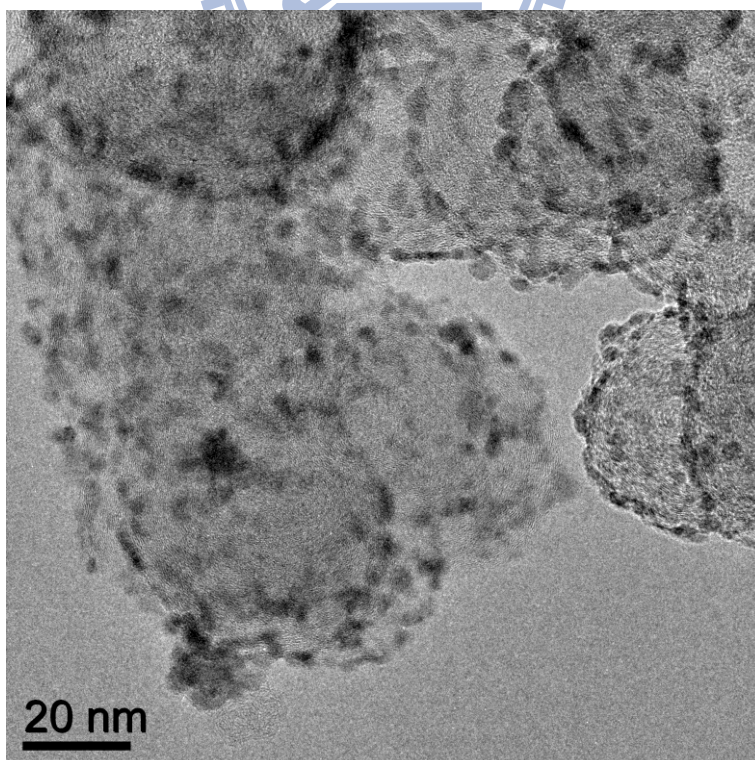


Figure 9. The TEM images for carbon supported Ru.





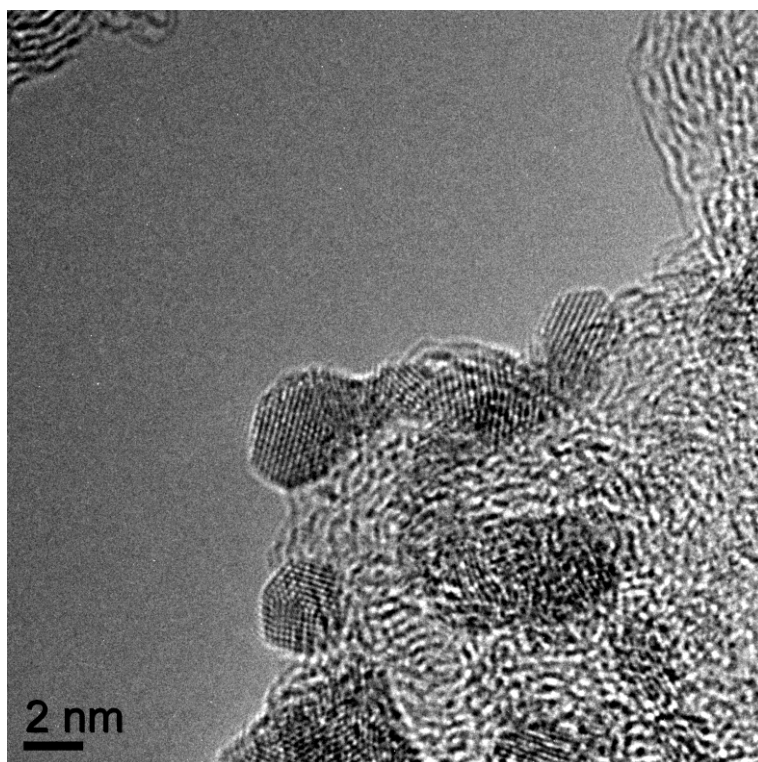
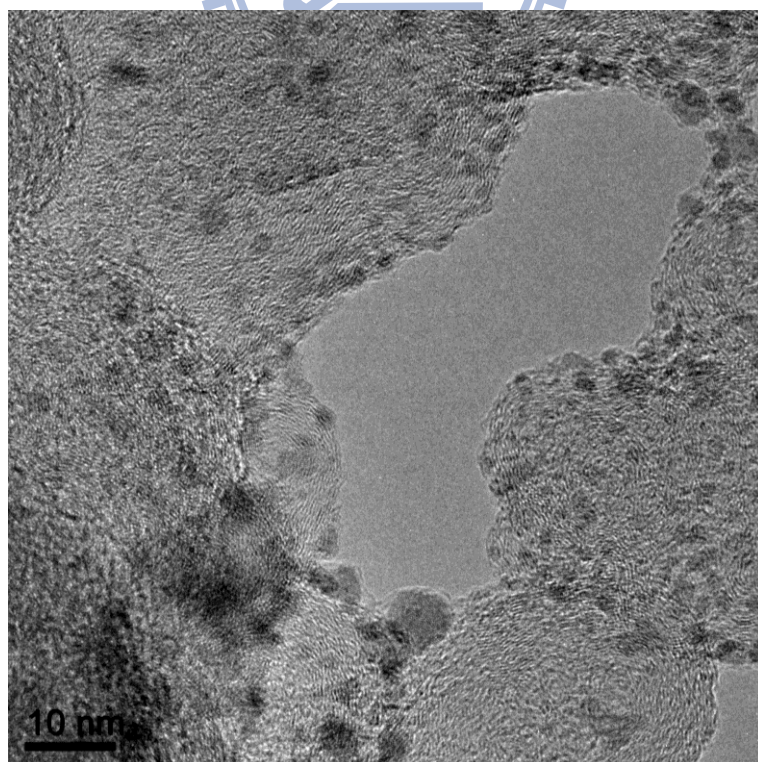


Figure 10. The TEM images for group A, Ru/C immersed with pH 1  $\text{H}_2\text{PtCl}_6$ .



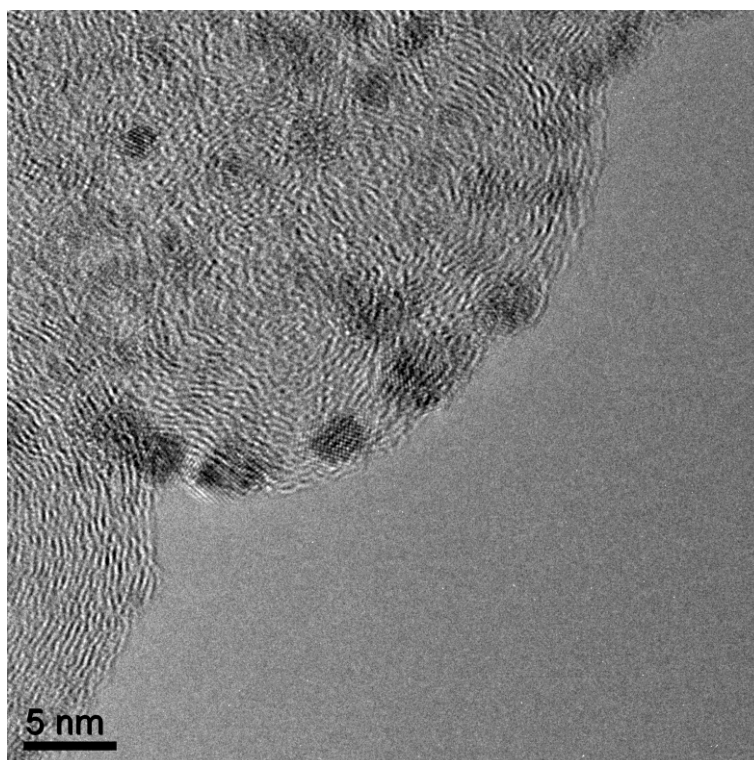
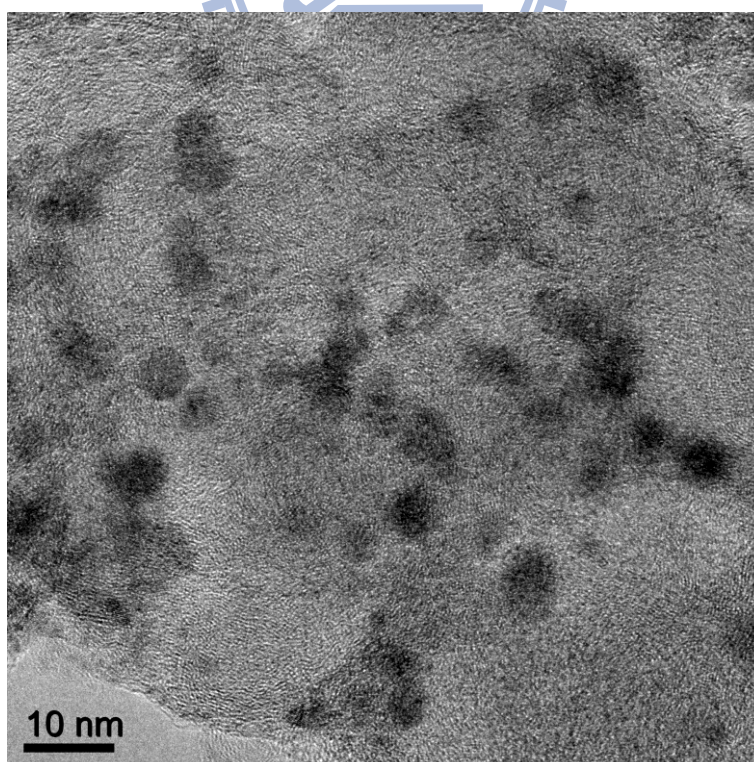


Figure 11. The TEM images for group B, Ru/C immersed with pH 2.2  $\text{H}_2\text{PtCl}_6$ .





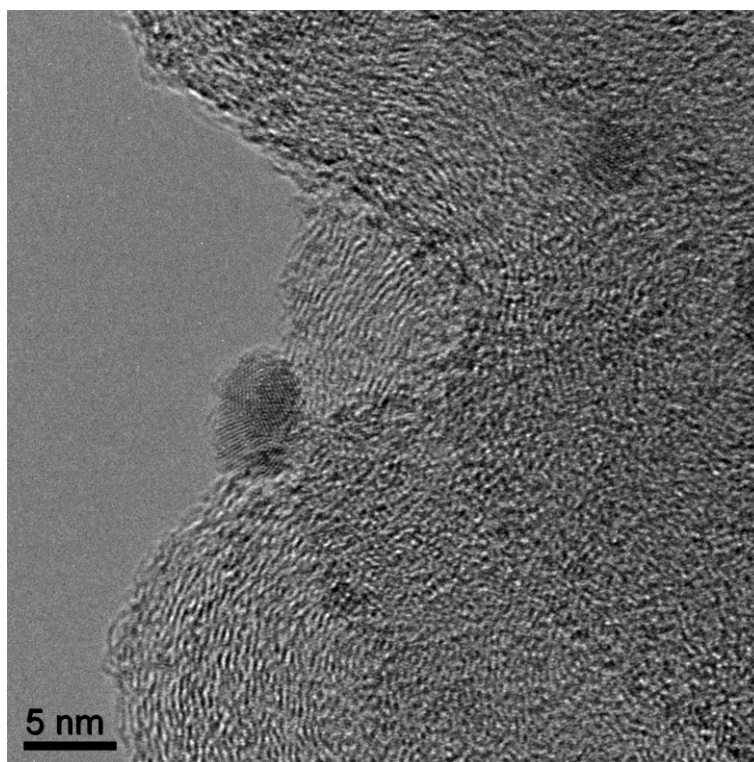


Figure 12. The TEM images for group C, Ru/C immersed with pH 8  $\text{H}_2\text{PtCl}_6$ .



The Ru K-edge XANES spectra for reference group are shown in Figure 13. After the immersion of perchloric acid (pH 1), de-ionized water (pH7.0) and potassium hydroxide (pH 8), Ru nanoparticles were oxidized based on the energy shift of the edge jump. The oxidation states of as-immersed Ru nanoparticles under various baths were similar. In addition, those oxidation states were between 0 to +4 according to the energy shifts which were located between that of  $\text{RuO}_2$  and metallic Ru powder (reference). The slight elevation for the oxidation states of Ru nanoparticles during the immersion was reasonably attributed to both contribution of water adsorption and oxide formation at the surface of Ru nanoparticles occurring together [18]. On the other hand, the oxide formation at the surface of Ru nanoparticles provided moderate protection against further

dissolution. After extended immersion, the Ru nanoparticles maintained their stability and sizes.

Figure 14 exhibits the Ru K-edge XANES spectra of group A. The oxidation states of Ru nanoparticles were similar for those immersed by various pH values of hexachloroplatinic acids. Interestingly, the oxidation states of group A Ru nanoparticles were approximately identical to that of reference group. These results confirmed that Ru maintained identical oxidation state during the displacement reaction by Pt atoms. Therefore, we assumed that the Ru species with higher oxidation states somehow left the surface in the form of dissolved complexes into the immersion baths. Similarly, the reduction process of Pt ions from the immersion baths onto the Ru nanoparticles could be assumed to include the formation of oxidized Ru and its subsequent dissolution. The Ru K-edge XANES for group B is exhibited in Figure 15. Similar results were obtained as group A even with a hydrogen reduction on the Ru nanoparticles. However, due to the reduced surface and the removal of surface oxides of Ru nanoparticles, a relatively stronger reduction driving force was provided for group B than group A. Therefore, the Pt species deposited on group B revealed lower oxidation states compared with group A. The Ru K-edge XANES for group C is shown in Figure 16. The hydrogen reduction treatment was applied after the immersion of Ru nanoparticles into hexachloroplatinic acids with various pH values. The oxidation states were not completely reduced to 0 like metallic Ru. This inevitable oxidation of Ru might be attributed to the oxygen-containing groups on the surface of functionalized carbon supports [19].

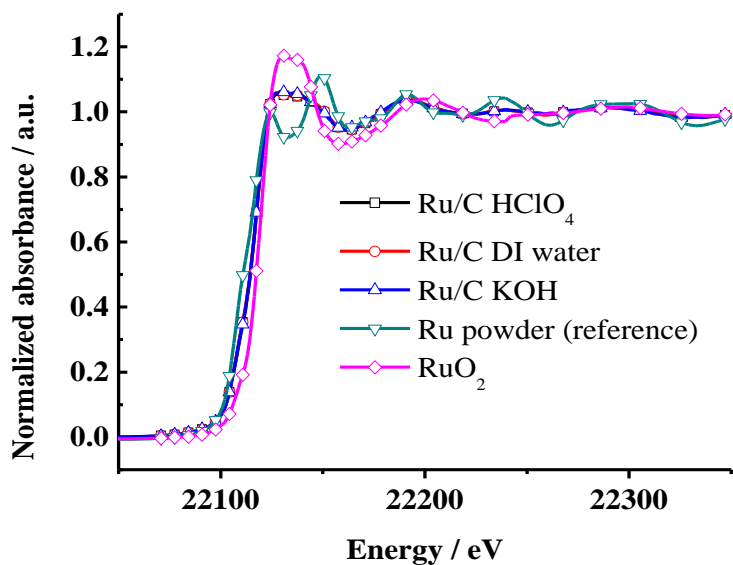


Figure 13. Ru K-edge XANES spectra of Ru metallic powder, RuO<sub>2</sub>, Ru/C immersed with HClO<sub>4</sub>,

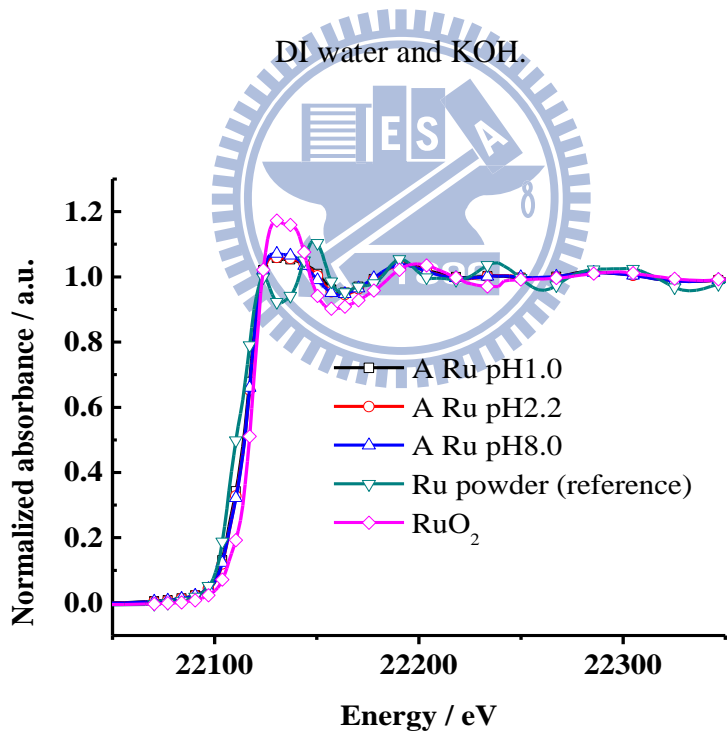


Figure 14. Ru K-edge XANES spectra of Ru metallic powder, RuO<sub>2</sub>, Ru/C immersed with pH 1, pH 2.2 and pH 8 H<sub>2</sub>PtCl<sub>6</sub> (group A).

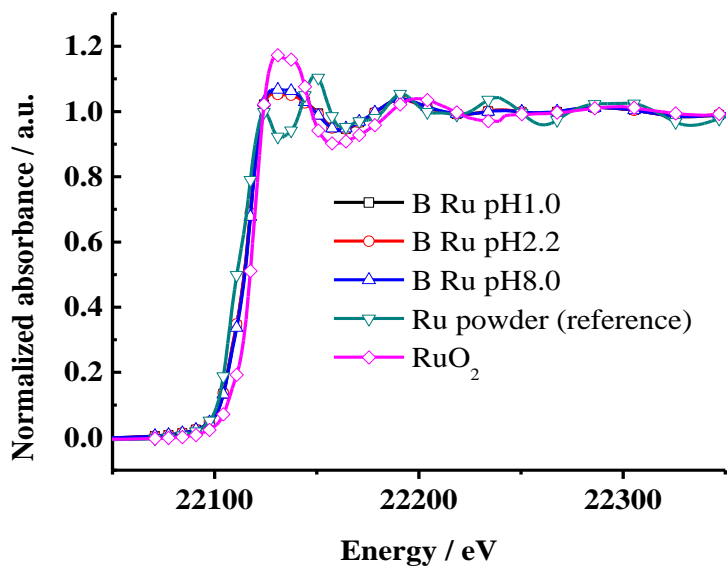


Figure 15. Ru K-edge XANES spectra of Ru metallic powder, RuO<sub>2</sub>, hydrogen reduced Ru/C immersed with pH 1, pH 2.2 and pH 8 H<sub>2</sub>PtCl<sub>6</sub> (group B).

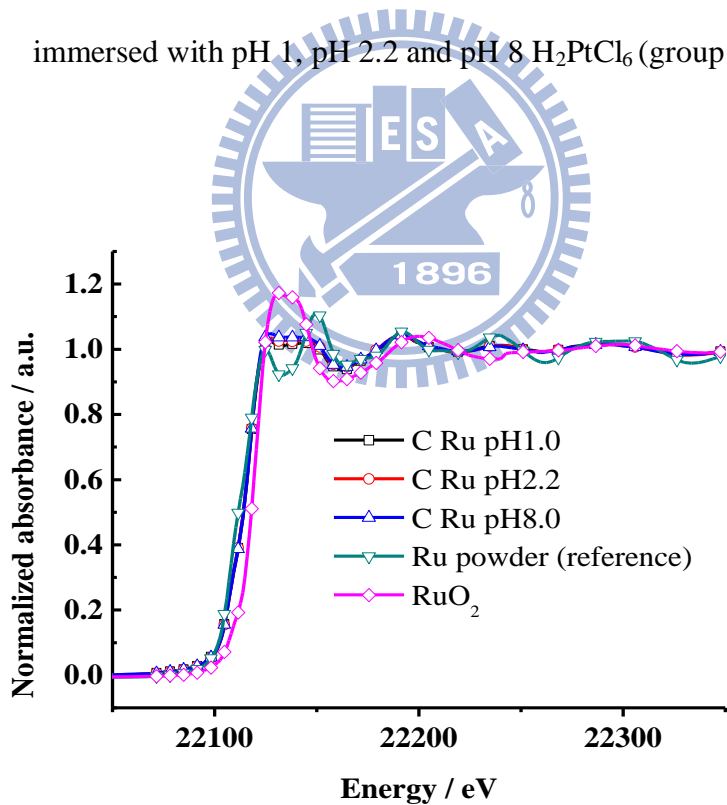


Figure 16. Ru K-edge XANES spectra of Ru metallic powder, RuO<sub>2</sub>, Ru/C immersed with pH 1, pH 2.2 and pH 8 H<sub>2</sub>PtCl<sub>6</sub> and followed by hydrogen reduction (group C).

The Ru K-edge Fourier transform EXAFS spectra for reference group, group A, group B, and group C are shown in Figure 17 to 20, respectively. The peaks at 1.6 Å and 2.3 Å (without phase correction) corresponded to the Ru-O bond and Ru-Ru bond at the first shell coordination. The EXAFS fitting results were summarized in table 3. For reference group, the coordination numbers of Ru-O of all immersion baths are around 2. The bonding between Ru and O was attributed to the formation of oxide layer on Ru nanoparticles caused by the immersion. Unfortunately, the fitting results of Ru which were immersed into H<sub>2</sub>PtCl<sub>6</sub> baths, group A, and group B, did not reveal any Ru-Pt coordination. As a result, the deposition of Pt on Ru was inconclusive from these EXAFS fittings. Nevertheless, once the hydrogen reduction was applied after the immersion as group C, Ru-Pt coordination numbers of 1.33, 1.08 and 0.82 were obtained for pH 1, pH 2.2 and pH 8 hexachloroplatinic acid immersion baths. EXAFS fitting results for group C also confirmed the presence of Ru-Pt bonding. This suggested that during the displacement reaction, Pt atoms were not deposited to Ru directly. Based on previous research by Hu et al. [46], the Ru might exist as bridged-oxygen oxide. The bridged-oxygen was expected to connect Pt to Ru. This may explain why the Ru-O was the predominant bonding species after the displacement reaction of Ru by Pt. This is because the Ru-O-Pt was formed instead of Ru-Pt on the surface of Ru nanoparticles. As expected, the Ru-Pt coordination was established as long as bridged-oxygen was removed.

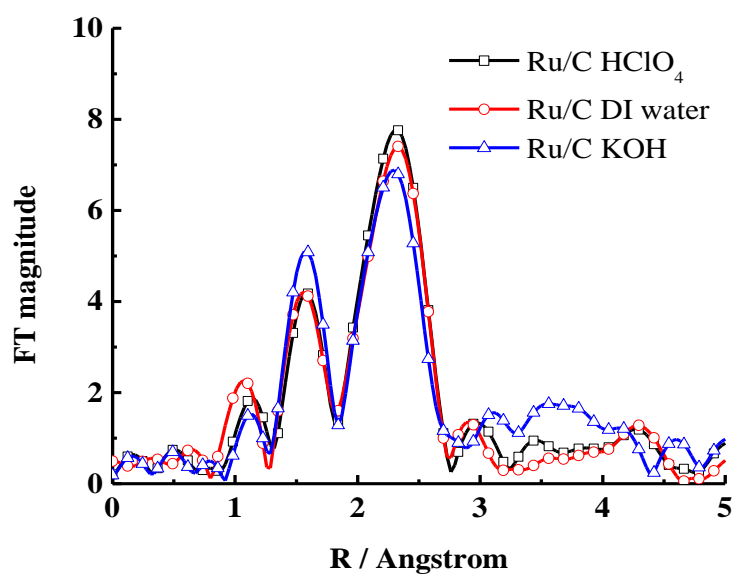


Figure 17. Ru K-edge EXAFS spectra of Ru/C immersed with HClO<sub>4</sub>, DI water and KOH.

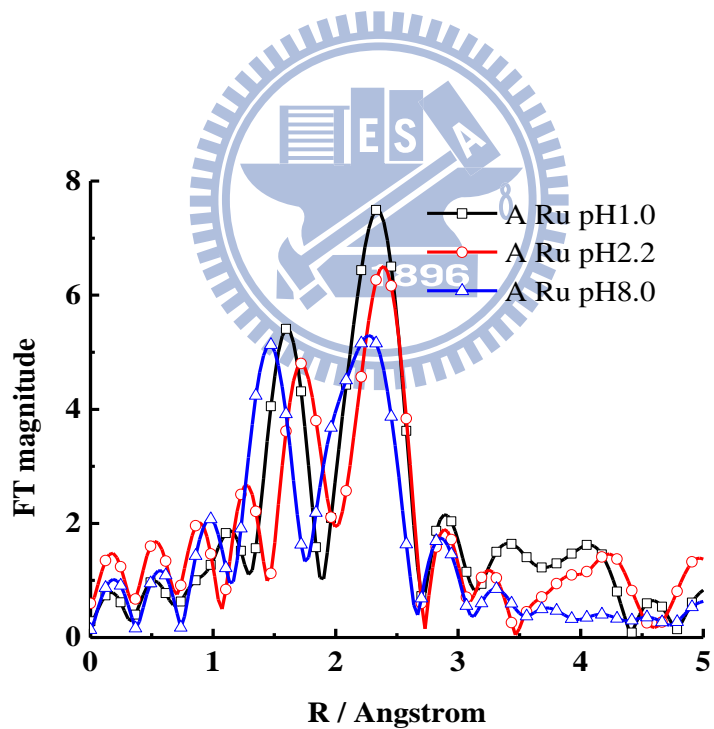


Figure 18. Ru K-edge EXAFS spectra of Ru/C immersed with pH 1, pH 2.2 and pH 8 H<sub>2</sub>PtCl<sub>6</sub> (group A).



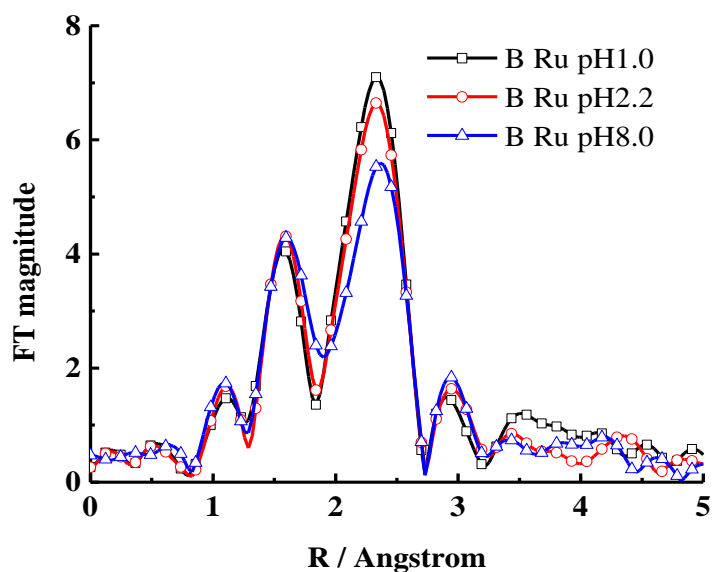


Figure 19. Ru K-edge EXAFS spectra of hydrogen reduced Ru/C immersed with pH 1, pH 2.2 and

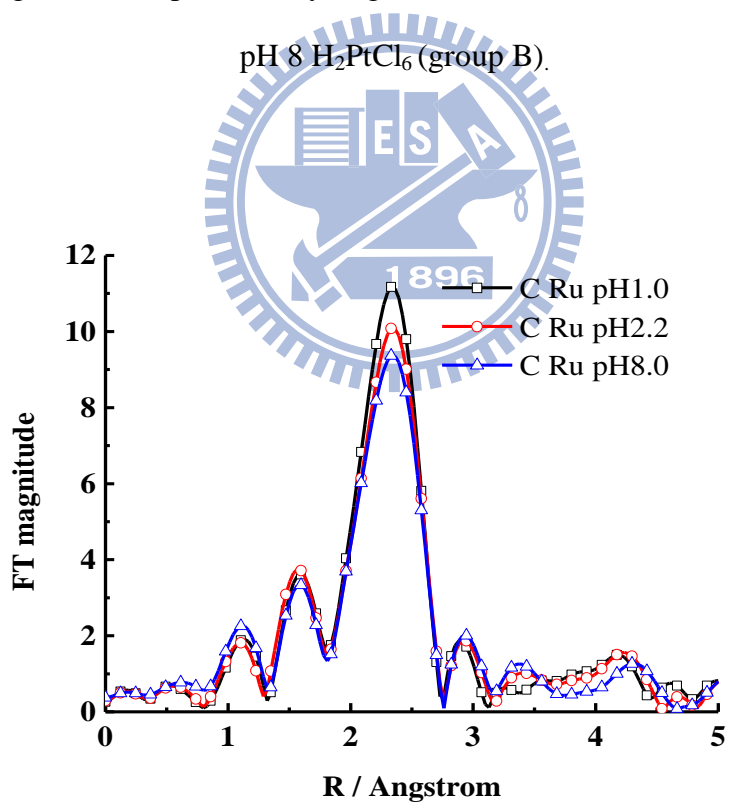


Figure 20. Ru K-edge EXAFS spectra of Ru/C immersed with pH 1, pH 2.2 and pH 8  $\text{H}_2\text{PtCl}_6$  and followed by hydrogen reduction (group C).

Table 3

The fitting results from the analysis of Ru K-edge EXAFS spectra.

|                        | Path  | Coordination<br>number, N | Bond<br>distance, R<br>(Å) | Inner potential<br>shift, $\Delta E_0$<br>(eV) | Debye-Waller<br>factor, $\Delta\sigma_j^2$<br>( $\times 10^{-3} \text{ \AA}^2$ ) |
|------------------------|-------|---------------------------|----------------------------|--|--|
| Ru/C HClO <sub>4</sub> | Ru-O  | 1.95                      | 2.04                       | -5.45  | 5.43   |
|                        | Ru-Ru | 3.64                      | 2.67                       | -9.92  | 7.29   |
| Ru/C DI<br>water       | Ru-O  | 1.99                      | 2.04                       | -4.36  | 5.41   |
|                        | Ru-Ru | 3.95                      | 2.67                       | -10.4  | 7.98   |
| Ru/C KOH               | Ru-O  | 1.94                      | 2.04                       | -6.15  | 3.32   |
|                        | Ru-Ru | 3.28                      | 2.67                       | -12.05   | 7.45   |
| A pH 1                 | Ru-O  | 1.23                      | 2.05                       | -0.55  | 0.13   |
|                        | Ru-Ru | 4.06                      | 2.67                       | -7.35  | 7.02   |
| A pH 2.2               | Ru-O  | 1.33                      | 2.07                       | -1.56  | 0.46   |
|                        | Ru-Ru | 4.28                      | 2.68                       | -7.10  | 8.26   |
| A pH 8                 | Ru-O  | 1.99                      | 2.02                       | -7.46  | 1.78   |
|                        | Ru-Ru | 4.08                      | 2.65                       | -12.88   | 7.03   |
| B pH 1                 | Ru-O  | 1.17                      | 2.03                       | -6.82  | 2.17   |
|                        | Ru-Ru | 3.98                      | 2.66                       | -10.41   | 7.02   |
| B pH 2.2               | Ru-O  | 1.78                      | 2.03                       | -11.14   | 3.72   |
|                        | Ru-Ru | 4.15                      | 2.67                       | -10.07   | 7.62   |
| B pH 8                 | Ru-O  | 2.07                      | 2.03                       | -6.99  | 4.46   |
|                        | Ru-Ru | 4.10                      | 2.67                       | -9.03  | 8.52   |
| C pH 1                 | Ru-O  | 1.07                      | 2.05                       | -6.54  | 4.23   |
|                        | Ru-Ru | 5.24                      | 2.69                       | -3.71  | 6.70   |

|          |       |      |      |        |      |
|----------|-------|------|------|--------|------|
|          | Ru-Pt | 1.33 | 2.71 | -9.44  | 5.91 |
|          | Ru-O  | 1.36 | 2.05 | -5.03  | 5.30 |
| C pH 2.2 | Ru-Ru | 5.12 | 2.69 | -4.14  | 7.20 |
|          | Ru-Pt | 1.08 | 2.70 | -13.59 | 6.62 |
|          | Ru-O  | 1.41 | 2.05 | -0.47  | 6.96 |
| C pH 8   | Ru-Ru | 4.54 | 2.69 | -3.62  | 6.91 |
|          | Ru-Pt | 0.82 | 2.71 | -8.24  | 5.64 |

Figure 21 demonstrates the Pt L<sub>3</sub>-edge XANES spectra of hexachloroplatinic acid adjusted to various pH values. The large peak at the absorption edge was attributed to 2p<sub>3/2</sub> to 5d electronic transition of Pt which is also known as white line [10, 47]. The white line intensity is able to provide information on the oxidation state of Pt due to its correspondence to d-band vacancy. A larger of the white line intensity, refers less d-band is occupied. That is, a high intensity white line is obtained for the Pt with a high oxidation state. Pt ions in hexachloroplatinic acids with various pH values revealed high white lines intensity similar due to the +4 oxidation number in Figure 16. For the white line of metallic Pt foil, its low intensity was designated as the 0 oxidation step.

For Pt atoms that were deposited onto Ru nanoparticles via the displacement reaction, their oxidation states can be observed in Figure 22. The Pt atoms that were deposited onto Ru nanoparticles with the immersion bath of hexachloroplatinic acid adjusted to pH 1 were partially reduced. For pH 2.2, although the oxidation state was slightly higher than that of pH 1, the partial reduction was observed. However, the Pt was nearly reduced for pH 8 based on its white line as high as that of Pt ions in hexachloroplatinic acid. A reasonable assumption could be adopted as physical adsorption for Pt ions onto Ru nanoparticles for the case of pH 8. In Figure 23, the white line intensities were generally lower than that in Figure 22. This result implied that for hydrogen

reduced Ru nanoparticle before immersion, group B, the Pt atoms were reduced even more compare with group A. Since the deposition through displacement reaction was expected to rely greatly on the surface, the hydrogen pretreatment that eliminated the surface oxides of Ru nanoparticles demonstrated clear evidence over reduced oxidation states of Pt atoms. In Figure 24, the intensities of white lines for group C were nearly as small as Pt foil because of the final hydrogen reduction. Nevertheless, the oxidation states were slightly higher for pH 1 and pH 2.2 than that of pH 8. This result indicated that sub-monolayer Pt for pH 1 and pH 2.2 facilitated each Pt atom to be a surface atom. For pH 8, the formation of Pt cluster might lead to a lower oxidation state due to the existence of protected inner Pt atoms.

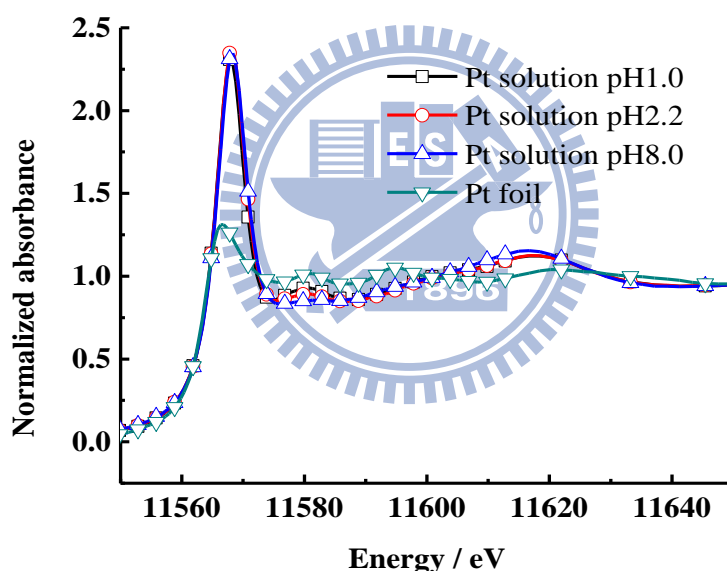


Figure 21. Pt L<sub>3</sub>-edge XANES spectra of Pt foil, H<sub>2</sub>PtCl<sub>6</sub> solution adjusted to pH 1, pH 2.2 and pH

8.

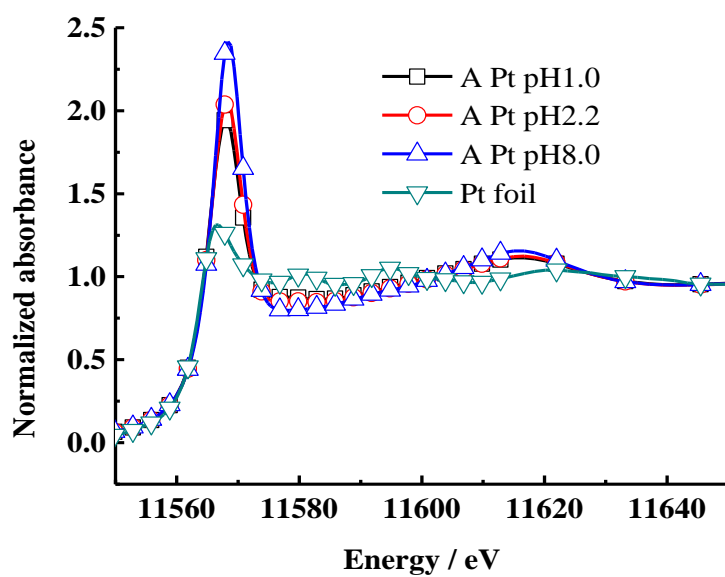


Figure 22. Pt L<sub>3</sub>-edge XANES spectra of Pt foil, Ru/C immersed with pH 1, pH 2.2 and pH 8

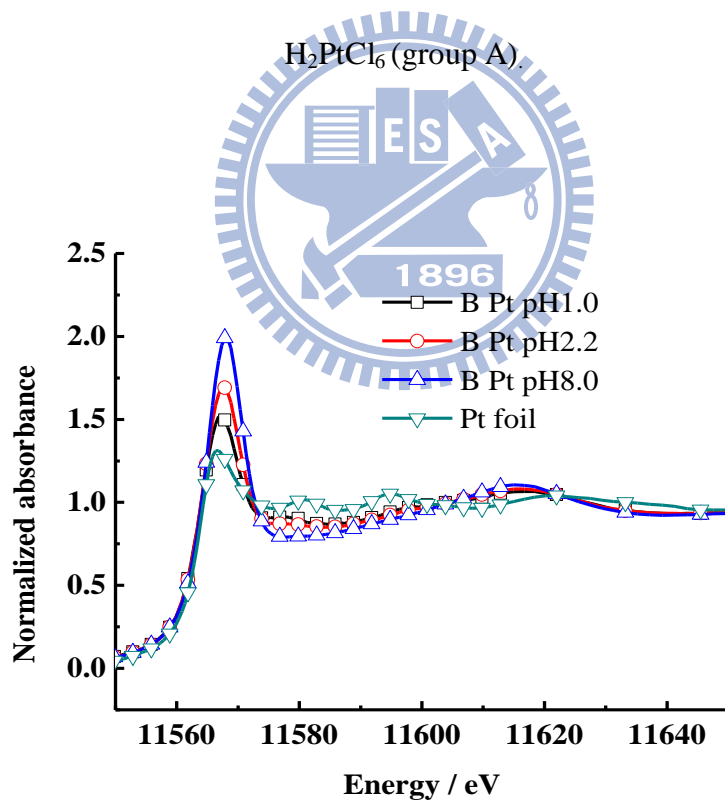


Figure 23. Pt L<sub>3</sub>-edge XANES spectra of Pt foil, hydrogen reduced Ru/C immersed with pH 1, pH 2.2 and pH 8 H<sub>2</sub>PtCl<sub>6</sub> (group B).

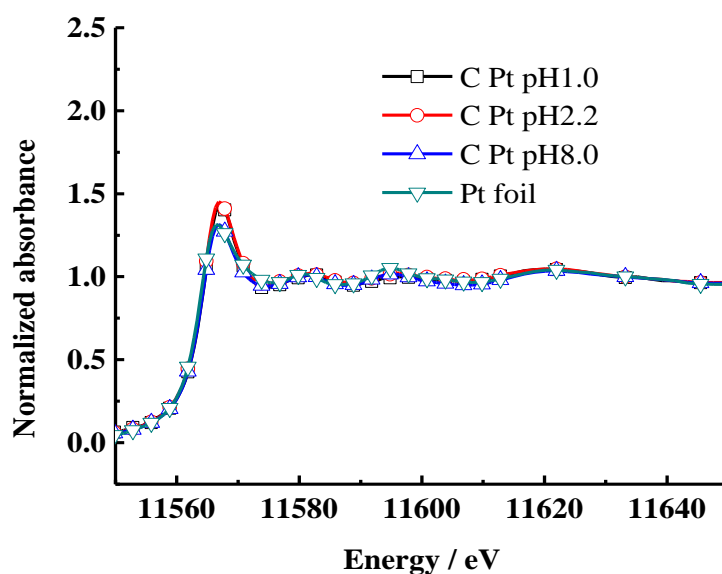


Figure 24. Pt L<sub>3</sub>-edge XANES spectra of Pt foil, Ru/C immersed with pH 1, pH 2.2 and pH 8 H<sub>2</sub>PtCl<sub>6</sub> and followed by hydrogen reduction (group C).

The Pt L<sub>3</sub>-edge Fourier transform EXAFS spectra for hexachloroplatinic acids, group A, group B and group C are shown in Figure 25 to 28, respectively. In Figure 25 to 27, the peaks at 1.7 Å and 2.0 Å (without phase correction) correspond to the Pt-O bond and Pt-Cl bond at the first shell coordination, respectively. In Figure 28, the peaks at 2.1 Å and 2.7 Å (without phase correction) correspond to the Pt-Ru bond and Pt-Pt bond at the first shell coordination, respectively. The EXAFS fitting results are summarized in table 4. Spieker et al. proposed that chloride ion ligands on the Pt complexes can be exchanged by hydroxide ligands or aqueous ligands due to the hydrolysis reaction in a thorough research of dilute hexachloroplatinic acid with various pH values [12]. Similar phenomena were observed in this work in which EXAFS fitting indicated a significant ligand change influenced by pH values based on Pt-Cl and Pt-O coordination number. The coordination numbers of Pt-O were 1.31, 1.65 and 3.58 for pH 1, pH 2.2 and pH 8 hexachloroplatinic acids, respectively. These results were coherent with Spieker et al in which ligand exchange by hydroxide or aqueous ligands with the increase of pH values. On the contrary,

EXAFS results determined that the coordination numbers of Pt-Cl were 4.69, 4.35 and 2.42 for pH 1, pH 2.2 and pH 8 hexachloroplatinic acids, respectively. In other words, the number of chloride ligands on the Pt complexes was reduced due to the hydrolysis reaction when pH value was increased. The variation of Pt ligand species should be responsible for causing notable influence toward the behavior of displacement reaction. For deposited Pt as group A, the sum of coordination number for Pt-O and Pt-Cl was decreased as presented in table 4, indicating the ligands were detached from the Pt complexes when Pt ions were reduced by Ru. Furthermore, under various pH values, the portion of Pt-O and Pt-Cl bonding for Pt on Ru was consistent to that in hexachloroplatinic acids. However, Pt-Ru bonding was not formed due to the bridged-oxygen structure. Similar outcome was obtained for group B. For the EXAFS fitting result in Figure 28, the coordination environment was changed dramatically due to the final hydrogen reduction which removed the bridged-oxygen. Table 4 also lists the coordination numbers of Pt-Ru which were 5.75, 4.23 and 3.21 for pH 1, pH 2.2 and pH 8 of group C, respectively. The results suggested that at low pH values, Pt ions were feasible of being reduced by Ru and replacing Ru atoms. It was obvious that the incorporation for the Pt into Ru nanoparticles occurred and contributed the Pt-Ru bonding as high as 5.75 and 4.23. At a high pH value, the Pt ions were merely physically adsorbed on the surface of Ru which its coordination number was further decreased. The coordination numbers of Pt-Pt are 1.71, 2.43 and 4.24 for pH 1, pH 2.2 and pH 8 of group C, respectively. At low pH values, the Pt atoms were assumed to form a sub-monolayer based on the relatively low Pt-Pt coordination number. On the contrary, the Pt clusters were expected to be formed for pH 8 consistent to the XRD results, giving a higher Pt-Pt coordination number.

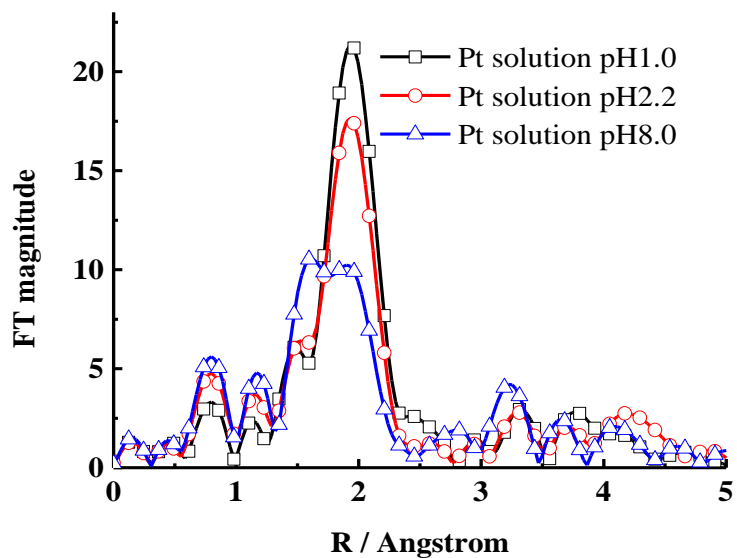


Figure 25. Pt L<sub>3</sub>-edge EXAFS spectra of H<sub>2</sub>PtCl<sub>6</sub> solution adjusted to pH 1, pH 2.2 and pH 8.

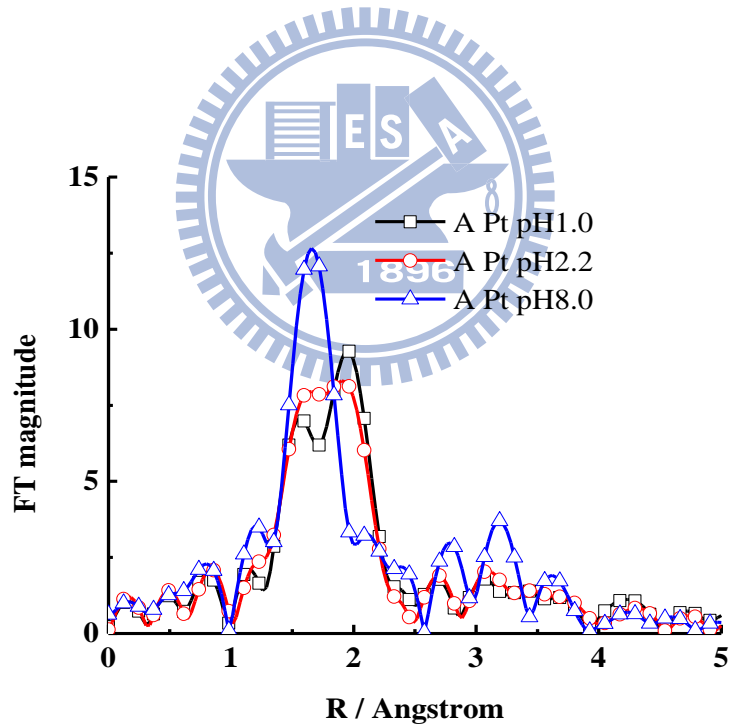


Figure 26. Pt L<sub>3</sub>-edge EXAFS spectra of Ru/C immersed with pH 1, pH 2.2 and pH 8 H<sub>2</sub>PtCl<sub>6</sub> (group A).



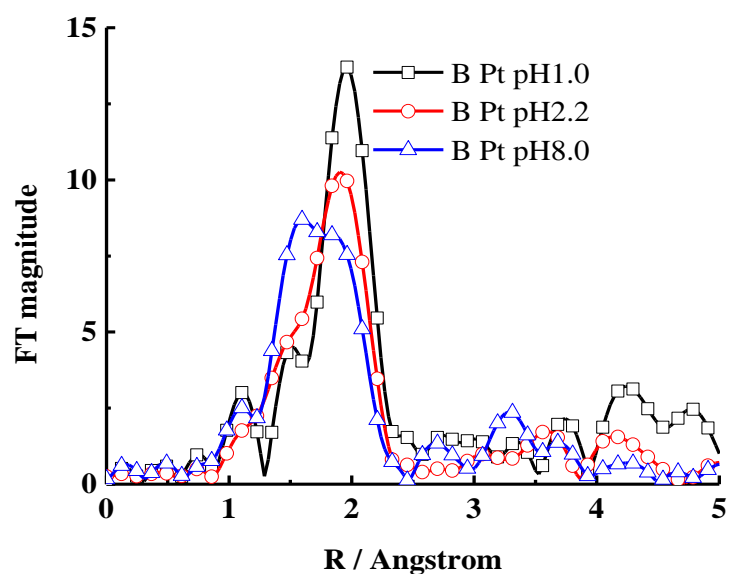


Figure 27. Pt L<sub>3</sub>-edge EXAFS spectra of hydrogen reduced Ru/C immersed with pH 1, pH 2.2 and

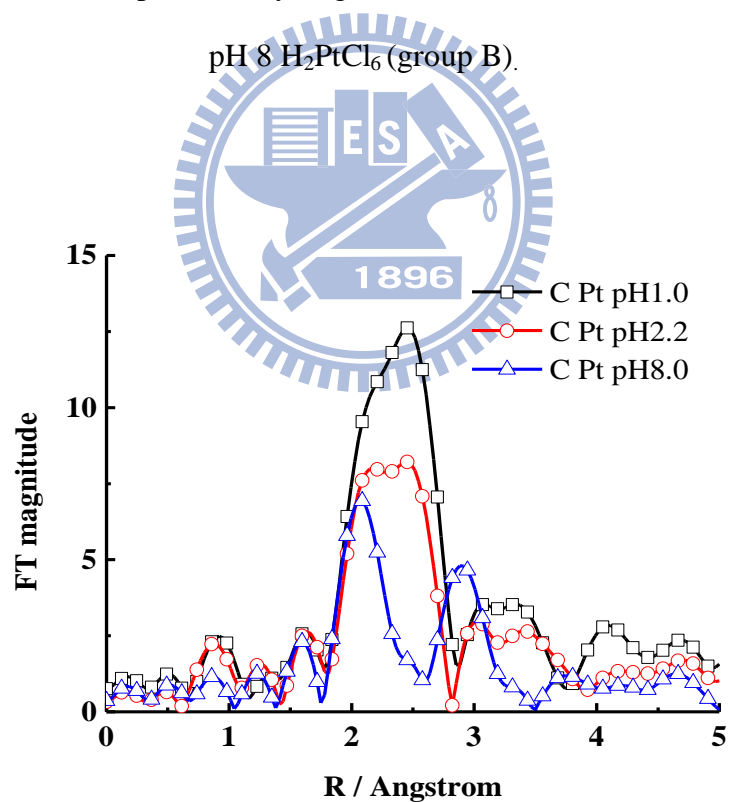


Figure 28. Pt L<sub>3</sub>-edge EXAFS spectra of Ru/C immersed with pH 1, pH 2.2 and pH 8 H<sub>2</sub>PtCl<sub>6</sub> and followed by hydrogen reduction (group C).

Table 4

The fitting results from the analysis of Pt L<sub>3</sub>-edge EXAFS spectra.

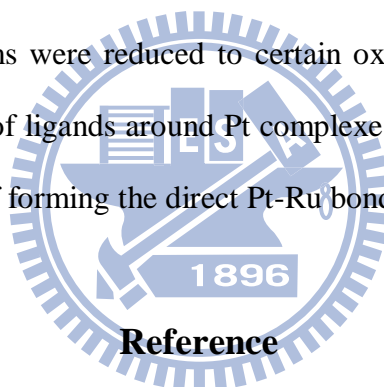
|                                     | Path  | Coordination<br>number, N | Bond<br>distance,<br>R (Å) | Inner potential<br>shift, $\Delta E_0$<br>(eV) | Debye-Walle<br>r factor, $\Delta\sigma_j^2$<br>( $\times 10^{-3} \text{ \AA}^2$ ) |
|-------------------------------------|-------|---------------------------|----------------------------|--|---|
| Hexachloroplatinic<br>acid (pH 1)   | Pt-O  | 1.31                      | 1.99                       | -2.14  | 2.79  |
|                                     | Pt-Cl | 4.69                      | 2.31                       | 10.16  | 2.79  |
| Hexachloroplatinic<br>acid (pH 2.2) | Pt-O  | 1.65                      | 1.99                       | -1.95  | 3.77  |
|                                     | Pt-Cl | 4.35                      | 2.31                       | 10.34  | 3.77  |
| Hexachloroplatinic<br>acid (pH 8)   | Pt-O  | 3.58                      | 1.99                       | 1.44   | 4.21  |
|                                     | Pt-Cl | 2.42                      | 2.31                       | 13.83  | 4.21  |
| A pH 1                              | Pt-O  | 1.95                      | 1.99                       | 7.26   | 1.78  |
|                                     | Pt-Cl | 1.69                      | 2.30                       | 9.16   | 1.57  |
| A pH 2.2                            | Pt-O  | 1.83                      | 2.00                       | 7.79   | 1.79  |
|                                     | Pt-Cl | 2.41                      | 2.30                       | 8.80   | 4.47  |
| A pH 8                              | Pt-O  | 3.66                      | 1.99                       | 3.73   | 2.42  |
|                                     | Pt-Cl | 1.83                      | 2.32                       | 18.35  | 11.17   |
| B pH 1                              | Pt-O  | 1.56                      | 2.01                       | 2.29   | 4.91  |
|                                     | Pt-Cl | 2.19                      | 2.32                       | 13.24  | 1.02  |
| B pH 2.2                            | Pt-O  | 1.67                      | 2.00                       | -4.94  | 3.19  |
|                                     | Pt-Cl | 2.94                      | 2.31                       | 12.52  | 1.99  |
| B pH 8                              | Pt-O  | 3.74                      | 2.01                       | 6.56   | 4.93  |
|                                     | Pt-Cl | 1.89                      | 2.32                       | 17.28  | 1.86  |
| C pH 1                              | Pt-Ru | 5.75                      | 2.71                       | 8.66   | 5.61  |
|                                     | Pt-Pt | 1.71                      | 2.76                       | 7.52   | 2.96  |

|          |       |      |      |      |      |
|----------|-------|------|------|------|------|
| C pH 2.2 | Pt-Ru | 4.23 | 2.71 | 7.69 | 5.60 |
|          | Pt-Pt | 2.43 | 2.76 | 8.65 | 4.82 |
| C pH 8   | Pt-Ru | 3.21 | 2.71 | 6.69 | 6.25 |
|          | Pt-Pt | 4.24 | 2.75 | 7.26 | 4.66 |

By summarizing the analytical results from XRD, ICP-MS, TEM, EDX and XAS spectra, the mechanism of Pt displacement reaction on Ru nanoparticles is described as follows. Pt ions were reduced by metallic Ru nanoparticles accompanied by the dissolution of Ru atoms at the surface. The dissolution of Ru atoms could be resulted from being replaced by Pt. Meanwhile, the formation of Ru oxide layer on the surface of it nanoparticle took place during the immersion into aqueous baths which eventually terminated the displacement reaction. The oxide layer prevented Ru from further dissolving and the reduction of Pt ions. The pH values of hexachloroplatinic acid played an essential role for the behavior of displacement reaction. Furthermore, two factors should be taken into consideration that various ligands around Pt complexes and extent of Ru dissolution in acidic/basic aqueous solvents. The deposition for Pt on Ru was formed through the bridged-oxygen instead of direct Pt-Ru bonding.

## Chapter 5 Conclusions

The mechanism of Pt displacement reaction on the Ru was investigated by immersing carbon supported Ru nanoparticles into hexachloroplatinic acids with various pH values and conducting hydrogen reduction before or after the immersion. XRD patterns suggested that the Ru hcp crystal structure was expanded slightly after Pt incorporation. ICP-MS indicated that the dissolution of Ru was mostly caused by the displacement by Pt atoms. TEM images revealed a uniform distribution of Pt deposited Ru with particle sizes around 2 to 3 nm. EDX confirmed that more Pt ions in acidic environment could be reduced by Ru, a result consistent with ICP-MS. Finally, the XAS analysis including XANES data and EXAFS fitting provided detailed displacement mechanism. Pt atoms were reduced to certain oxidation states or merely physically adsorbed depending on the types of ligands around Pt complexes. Pt atoms were deposited onto Ru through bridged-oxygen instead of forming the direct Pt-Ru bonding during displacement reaction.



### Reference

- [1] Wasmus S, Kuver A. Methanol oxidation and direct methanol fuel cells: a selective review. *J Electroanal Chem.* 1999;461(1-2):14-31.
- [2] Arico AS, Shukla AK, Kim H, Park S, Min M, Antonucci V. An XPS study on oxidation states of Pt and its alloys with Co and Cr and its relevance to electroreduction of oxygen. *Appl Surf Sci.* 2001;172(1-2):33-40.
- [3] Lamy C, Léger J-M, Srinivasan S. Direct Methanol Fuel Cells: From a Twentieth Century Electrochemist's Dream to a Twenty-first Century Emerging Technology. 2002, p. 53-118.
- [4] Watanabe M, Motoo S. Electrocatalysis by ad-atoms: Part II. Enhancement of the oxidation of methanol on platinum by ruthenium ad-atoms. *J Electroanal Chem.* 1975;60(3):267-73.

- [5] Frelink T, Visscher W, van Veen JAR. On the role of Ru and Sn as promoters of methanol electro-oxidation over Pt. *Surface Science*. 1995;335:353-60.
- [6] Liu HS, Song CJ, Zhang L, Zhang JJ, Wang HJ, Wilkinson DP. A review of anode catalysis in the direct methanol fuel cell. *J Power Sources*. 2006;155(2):95-110.
- [7] Takasu Y, Fujiwara T, Murakami Y, Sasaki K, Oguri M, Asaki T, et al. Effect of structure of carbon-supported PtRu electrocatalysts on the electrochemical oxidation of methanol. *J Electrochem Soc*. 2000;147(12):4421-7.
- [8] Steigerwalt ES, Deluga GA, Cliffl DE, Lukehart CM. A Pt-Ru/graphitic carbon nanofiber nanocomposite exhibiting high relative performance as a direct-methanol fuel cell anode catalyst. *J Phys Chem B*. 2001;105(34):8097-101.
- [9] Lizcano-Valbuena WH, Paganin VA, Gonzalez ER. Methanol electro-oxidation on gas diffusion electrodes prepared with Pt-Ru/C catalysts. *Electrochimica Acta*. 2002;47(22-23):3715-22.
- [10] Fujiwara N, Yasuda K, Ioroi T, Siroma Z, Miyazaki Y. Preparation of platinum-ruthenium onto solid polymer electrolyte membrane and the application to a DMFC anode. *Electrochimica Acta*. 2002;47(25):4079-84.
- [11] Dickinson AJ, Carrette LPL, Collins JA, Friedrich KA, Stimming U. Preparation of a Pt-Ru/C catalyst from carbonyl complexes for fuel cell applications. *Electrochimica Acta*. 2002;47(22-23):3733-9.
- [12] Watanabe M, Uchida M, Motoo S. Preparation of Highly Dispersed Pt+Ru Alloy Clusters and the Activity for the Electrooxidation of Methanol. *J Electroanal Chem*. 1987;229(1-2):395-406.
- [13] Radmilovic V, Gasteiger HA, Ross PN. Structure and Chemical-Composition of a Supported Pt-Ru Electrocatalyst for Methanol Oxidation. *J Catal*. 1995;154(1):98-106.
- [14] Luna AMC, Camara GA, Paganin VA, Ticianelli EA, Gonzalez ER. Effect of thermal

treatment on the performance of CO-tolerant anodes for polymer electrolyte fuel cells. *Electrochem Commun.* 2000;2(4):222-5.

- [15] Hills CW, Mack NH, Nuzzo RG. The size-dependent structural phase behaviors of supported bimetallic (Pt-Ru) nanoparticles. *J Phys Chem B.* 2003;107(12):2626-36.
- [16] Liu YC, Qiu XP, Chen ZG, Zhu WT. A new supported catalyst for methanol oxidation prepared by a reverse micelles method. *Electrochem Commun.* 2002;4(7):550-3.
- [17] Zhang X, Chan KY. Water-in-oil microemulsion synthesis of platinum-ruthenium nanoparticles, their characterization and electrocatalytic properties. *Chem Mater.* 2003;15(2):451-9.
- [18] Solla-Gullón J, Vidal-Iglesias FJ, Montiel V, Aldaz A. Electrochemical characterization of platinum-ruthenium nanoparticles prepared by water-in-oil microemulsion. *Electrochimica Acta.* 2004;49(28):5079-88.
- [19] Adzic RR, Zhang J, Sasaki K, Vukmirovic MB, Shao M, Wang JX, et al. Platinum monolayer fuel cell electrocatalysts. *Top Catal.* 2007;46(3-4):249-62.
- [20] Brankovic SR, Wang JX, Adzic RR. Pt submonolayers on Ru nanoparticles - A novel low Pt loading, high CO tolerance fuel cell electrocatalyst. *Electrochem Solid St.* 2001;4(12):A217-A20.
- [21] Zhang J, Lima FHB, Shao MH, Sasaki K, Wang JX, Hanson J, et al. Platinum monolayer on nonnoble metal-noble metal core-shell nanoparticle electrocatalysts for O<sub>2</sub> reduction. *J Phys Chem B.* 2005;109(48):22701-4.
- [22] Zhang J, Vukmirovic MB, Sasaki K, Uribe F, Adzic RR. Platinum monolayer electro catalysts for oxygen reduction: effect of substrates, and long-term stability. *J Serb Chem Soc.* 2005;70(3):513-25.
- [23] Zhang JL, Vukmirovic MB, Xu Y, Mavrikakis M, Adzic RR. Controlling the catalytic activity of platinum-monolayer electrocatalysts for oxygen reduction with different substrates. *Angew*

Chem Int Edit. 2005;44(14):2132-5.

- [24] Sasaki K, Wang JX, Balasubramanian M, McBreen J, Uribe F, Adzic RR. Ultra-low platinum content fuel cell anode electrocatalyst with a long-term performance stability. *Electrochimica Acta*. 2004;49(22-23):3873-7.
- [25] Russell AE, Rose A. X-ray absorption Spectroscopy of low temperature fuel cell catalysts. *Chem Rev*. 2004;104(10):4613-35.
- [26] Koningsberger DC, Prins R. X-ray absorption : principles, applications, tech by D.C. Koningsberger and R. Prins: John Wiley & Sons; 1988.
- [27] Waszczuk P, Lu GQ, Wieckowski A, Lu C, Rice C, Masel RI. UHV and electrochemical studies of CO and methanol adsorbed at Pt/Ru surfaces, and reference to fuel cell catalysis. *Electrochimica Acta*. 2002;47(22-23):3637-52.
- [28] Yajima T, Uchida H, Watanabe M. In-situ ATR-FTIR spectroscopic study of electro-oxidation of methanol and adsorbed CO at Pt-Ru alloy. *Journal of Physical Chemistry B*. 2004;108(8):2654-9.
- [29] Desai S, Neurock M. A first principles analysis of CO oxidation over Pt and Pt<sub>66.7%</sub>Ru<sub>33.3%</sub> (111) surfaces. *Electrochimica Acta*. 2003;48(25-26):3759-73.
- [30] Ando YJ, Sasaki K, Adzic R. Electrocatalysts for methanol oxidation with ultra low content of Pt and Ru. *Electrochemistry Communications*. 2009;11(6):1135-8.
- [31] Wang RF, Li H, Feng HQ, Wang H, Lei ZQ. Preparation of carbon-supported core@shell PdCu@PtRu nanoparticles for methanol oxidation. *Journal of Power Sources*. 2010;195(4):1099-102.
- [32] Sasaki K, Wang JX, Balasubramanian M, McBreen J, Uribe F, Adzic RR. Ultra-low Pt content fuel cell anode electrocatalyst with a long-term performance stability. *Electrochimica Acta*. 2004;49(22-23):3873-7.
- [33] Brankovic SR, McBreen J, Adzic RR. Spontaneous deposition of Pt on the Ru(0001) surface.

Journal of Electroanalytical Chemistry. 2001;503(1-2):99-104.

- [34] Brankovic SR, Wang JX, Adzic RR. Pt submonolayers on Ru nanoparticles - A novel low Pt loading, high CO tolerance fuel cell electrocatalyst. *Electrochemical and Solid State Letters*. 2001;4(12):A217-A20.
- [35] Brankovic SR, Wang JX, Zhu Y, Sabatini R, McBreen J, Adzic RR. Electrosorption and catalytic properties of bare and Pt modified single crystal and nanostructured Ru surfaces. *Journal of Electroanalytical Chemistry*. 2002;524:231-41.
- [36] Citrin PH, Wertheim GK. PHOTOEMISSION FROM SURFACE-ATOM CORE LEVELS, SURFACE DENSITIES OF STATES, AND METAL-ATOM CLUSTERS - A UNIFIED PICTURE. *Physical Review B*. 1983;27(6):3176-200.
- [37] Manandhar S, Kelber JA. Spontaneous deposition of Pt and Ir on Ru: Reduction to intermediate oxidation states. *Electrochimica Acta*. 2007;52(15):5010-7.
- [38] Spieker WA, Liu J, Miller JT, Kropf AJ, Regalbuto JR. An EXAFS study of the co-ordination chemistry of hydrogen hexachloroplatinate(IV) 1. Speciation in aqueous solution. *Applied Catalysis a-General*. 2002;232(1-2):219-35.
- [39] Zhang GX, Sun SH, Yang DQ, Dodelet JP, Sacher E. The surface analytical characterization of carbon fibers functionalized by H<sub>2</sub>SO<sub>4</sub>/HNO<sub>3</sub> treatment. *Carbon*. 2008;46(2):196-205.
- [40] Ravel B, Newville M. ATHENA, ARTEMIS, HEPHAESTUS: data analysis for X-ray absorption spectroscopy using IFEFFIT. *Journal of Synchrotron Radiation*. 2005;12:537-41.
- [41] Newville M. IFEFFIT : interactive XAFS analysis and FEFF fitting. *Journal of Synchrotron Radiation*. 2001;8(2):322-4.
- [42] Lee H-Y, Wu T-B, Lee J-F. X-ray absorption spectroscopic studies of sputter-deposited LaNiO<sub>3</sub> thin films on Si substrate. *Journal of Applied Physics*. 1996;80(4):2175-80.
- [43] Rehr JJ, Albers RC. Theoretical approaches to x-ray absorption fine structure. *Reviews of Modern Physics*. 2000;72(3):621.



- [44] Sugawara Y, Yadav AP, Nishikata A, Tsuru T. EQCM study on dissolution of Ru in sulfuric acid. *Journal of the Electrochemical Society*. 2008;155(9):B897-B902.
- [45] Liu DG, Lee JF, Tang MT. Characterization of Pt-Ru/C catalysts by X-ray absorption spectroscopy and temperature-programmed surface reaction. *Journal of Molecular Catalysis a-Chemical*. 2005;240(1-2):197-206.
- [46] Hu CC, Chiang HR, Wang CC. Electrochemical and structural investigations of oxide films anodically formed on Ru-plated titanium electrodes in sulfuric acid. *Journal of Solid State Electrochemistry*. 2003;7(8):477-84.
- [47] Meitzner G, Via GH, Lytle FW, Sinfelt JH. ANALYSIS OF X-RAY ABSORPTION-EDGE DATA ON METAL-CATALYSTS. *Journal of Physical Chemistry*. 1992;96(12):4960-4.

